Large-scale boudinage of late Miocene platform series triggered by margin collapse during the messinian salinity crisis (Ibiza island, Spain)

F. Odonne, A. Maillard, C. Lézin, F. Chanier, V. Gaullier, D. Guillaume

LARGE-SCALE BOUDINAGE OF LATE MIOCENE PLATFORM SERIES TRIGGERED BY MARGIN COLLAPSE DURING THE MESSINIAN SALINITY CRISIS (IBIZA ISLAND, SPAIN)

Odonne F.[a,1], Maillard A.[a], Lézin C.[a], Chanier F.[b], Gaullier V.[b] and Guillaume D.[c]

[a] Géosciences Environnement Toulouse (GET), Observatoire Midi-Pyrénées, Université de Toulouse, CNRS, IRD, UMR 5563, 14 Avenue E. Belin, F-31400 Toulouse, France.

[b] Univ. Lille, CNRS, Univ. Littoral Côte d'Opale, UMR 8187, Laboratoire d'Océanologie et de Géosciences (LOG), F-59000 Lille, France.

[C] Univ. Lyon, UJM-Saint-Étienne, UCA, CNRS, IRD, LMV UMR 6524, F-42023, Saint-Étienne, France.

[1] Corresponding author: francis.odonne@get.omp.eu

ABSTRACT

In Ibiza Island, we show for the first time that the post-tectonic late Miocene deposits are locally deformed in synsedimentary large scale boudinage structures. The late Miocene series is composed of a carbonate rich Unit 1 that is overlaid by a clastic Unit 2 and a Unit 3 in which a basal oolite-rich deposit is distinguished from an upper stromatolite-rich part. The oolite-rich and competent layers of Unit 3 are dissected into large rectangular to barrel-shape boudins that indicate a multidirectional extension. The separation of the blocks develops significantly northward revealing a stretching increase in a seaward direction that could have been favored by sliding of the distal part of the underlying marly unit over the clays. Along and in between the boudins, the laminated layers form soft-sediment syncline folds. The progressive bending of these laminated layers created spaces that were filled with calcite crystal wedges, providing evidence for large fluid circulation during deformation. Microthermometry on fluid inclusions in these calcite crystals revealed growth-temperatures ranging from 190 to 260°C. This high recrystallization rate is an indication of important fluid circulation during deformation processes. Besides, the progressive infill of paleosols over some of the synsedimentary synclines indicates that deformation was a slow process during the emersion of the series. And the subaerial Messinian channels location in the topographic depressions formed by the boudinage of the late Miocene series confirms that the deformation and sliding occurred during the relative emersion associated with the Messinian Salinity Crisis. We thus interpret the boudinage as resulting from the destabilization of a still soft

carbonate platform whose sliding has been helped substantially by the injection of relatively hot fluids. This work provides an onland evidence for extensional collapse during the Messinian sea-level drawdown.

Keywords: Ibiza, late Miocene, Messinian Salinity Crisis, boudinage, soft-sediment deformation.

1. Introduction

In Ibiza Island (Figs. 1 & 2), the late Miocene series are mostly composed of calcareous rocks (Rangheard, 1971; Durand-Delga et al., 1993) and affected by synsedimentary structures recognized by Simó Marfa (1982). A succession of gentle folds and segmented layers (boudinage) deforms the late Miocene series that can be observed in the north-eastern part of the island, around Portinatx (Fig. 3). These sedimentary rocks are interpreted in the Messinian Salinity Crisis (MSC) context occurring at the end of the Miocene, and compared to well-known deposits processes and coeval to the crisis. The Ibiza late Miocene limestones are well exposed. They were deposited in the platform topographic lows. They appear to be poorly affected by thin-skinned tectonics compared to the Mesozoic to middle Miocene formations elsewhere on the island that recorded the Betic orogeny.

The structures around Portinatx may result from “soft-sediment deformation”. The soft-sediment deformation mainly results in the relative displacement of grains in unconsolidated sediments (Allen, 1982; Maltman, 1984). Nevertheless, recognition of soft-sediment deformation processes and trigger mechanisms is often a difficult process (Moretti and Sabato, 2007), particularly in carbonate rocks where the eodiagenetic cementation can occur very early after the period of deposit. In that case, fluid circulations or water escape structures indicate the occurrence of soft-sediment deformation (Lowe, 1975; Leeder, 1987; Owen, 1987). In the Miocene sediments, around Portinatx, the widespread recrystallization of the limestones and the great number of calcite veins in interbedded positions give evidence of such large circulation of fluids but it is not any proof of cold synsedimentary conditions. The comparison of the converging pictures of metamorphic rock structures and soft-sediment deformation structures (Ogata et al., 2016) provides substantial help to describe the structures. The complete lack of cleavage, of veins in the fold hinges and growth of metamorphic minerals, are clear indications of the occurrence of soft-sediment deformation. It is the case for the late Miocene limestones that have been gently deformed, but the conditions of the deformation structures have not been clearly defined.

The ductile deformation structures of the late Miocene series provide an opportunity to investigate the potential relationship between early deformation of the platform and the sea-level drawdown during the Messinian Salinity Crisis. We investigate those structures in order (i) to understand the formation of atypical boudinage and folding, (ii) to recognize the occurrence of soft-sediment deformation, (iii) to propose triggering mechanisms, (iv) to possibly relate them to the MSC event.

2. Geological context and methodology

2.1 Regional geodynamics of the Balearic Promontory

The Balearic Promontory is a continental rise (500 km-long, 120 km-wide, Fig. 1) that includes the Balearic Islands, surrounded by narrow platforms and steep slopes toward the basins. Although located between two extensional basins, the Valencia Basin to the north and the Algerian Basin to the south, the Balearic Islands result mostly from the compressional deformation associated with the Betic orogenic system that has been active by parts from Eocene to Miocene (Rangheard, 1971; Ramos Guerrero et al., 1989; Sanz De Galdeano, 1990; Roca, 2001) and belong to the External zones of the mountain range. The Betic thrusts are well expressed on Ibiza and Mallorca (Fourcade et al., 1982; Gelabert et al., 1992, 2004; Sàbat et al., 2011) as well as offshore in the Valencia Basin, in the lower slope domain of the islands (Maillard et al., 1992; Mauffret et al., 1992; Sàbat et al., 1997, 2011; Ethève et al., 2016). In Ibiza, Ethève et al., (2016) show that the extensional event responsible for the formation of the surrounding Valencia basin predates the Betic compression (middle Miocene).

Actually, the Balearic Promontory underwent an extensional event from the late Serravallian to Tortonian, notably expressed in the Palma graben in Mallorca (Roca and Guimera, 1992) and in offshore basins, possibly linked to post-orogenic collapse or / and to the westward translation of the Alboran domain, along the E. Baudot transform margin (Fig. 1) (e.g. Frizon de Lamotte et al., 1991; Mauffret et al., 2001; Platt et al., 2003; Platt et al., 2013; Driussi et al., 2015). Moreover, although the borders of the Balearic Promontory are considered as passive margins, gentle active deformation has been reported in the Alicante shelf, and in the Ibiza and Mallorca channels (Sabat et al., 1997; Alfaro et al., 2002; Maillard and Mauffret, 2013). In the Ibiza Channel, the abundance of mass failure structures also supports the occurrence of active tectonic processes and/or volcanism (Acosta et al., 2002; Lastras et al., 2004; Acosta et al., 2013). Cenozoic succession of compressional and extensional tectonic events is thus responsible for the complex structural setting of that area.

2.2 Mio-Pliocene context of Ibiza Island

Ibiza Island is mainly composed of Mesozoic rocks separated from the overlying marine late Oligocene conglomerate and Langhian nanno and planctonic rich marly turbidites (Durand-Delga et al., 1993; Rangheard et al., 2011). These Cenozoic deposits are involved in the orogenic deformation (Fourcade et al.,1982; Fontboté et al., 1990; Sàbat et al.,1997). In the NE part of Ibiza Island, the postorogenic transgressive deposits are late Miocene, composed of 3 marine units described by Simó-Marfa (1982) and attributed to the Tortonian with some uncertainties (Rangheard, 1971; Durand-Delga et al., 1993; Rangheard et al., 2011). It is topped by an erosion surface covered by marine then aeolian Plio-Pleistocene deposits (Simó-Marfa, 1982; Lezin et al., 2014; 2017). This erosion surface is related to the one affecting most of the Mediterranean margins, called the Margin Erosion Surface (MES) related to a high-amplitude drop of the sea level during the Messinian Salinity Crisis (Lofi et al., 2011). This short-term dramatic event occurred between 5.96 and 5.32 Ma (Gautier et al., 1994; Krijgsman et al., 1999). It resulted first in the deposit of evaporites in "shallow" peripheral basins (Primary Lower Gypsum); then evaporite precipitation shifted to the abyssal basins ("deep basin evaporites"), while subaerial erosion affected shallow areas and Mediterranean margins (CIESM, 2008; Ryan, 2008; Roveri et al., 2014). The MSC sea-level drawdown is thus responsible for incisions of deep fluvial canyons (Hsü et al., 1973; Clauzon et al., 1996; Rouchy and Caruso, 2006; Lofi et al., 2011), large transfer of sediments and margin collapse (Bache et al., 2009; Maillard et al., 2014; Cameselle and Urgeles, 2017). Unlike in Mallorca Island where Primary Gypsum in the Palma Bay reveals a shallow peripheral basin, there are no MSC-related evaporites in Ibiza Island but the crisis is recorded by the MES, that extends throughout the offshore Balearic margins (Fig. 2) until it turns to the deep basin evaporites in surrounding Valencia and Algerian abyssal basins (Driussi et al., 2014).

2.3 Methodology

High-resolution stratigraphic sections have been made in the different calas of NE Ibiza. In each section, the different units have been recognized and correlated over the studied area. A specific paper devoted to the high-resolution stratigraphy of the Miocene-Pliocene units is in preparation (Lezin C., personal communication). In the present paper, we show a synthetic stratigraphy of the area in figure 4. At the same time and over the same outcrops, structural observations and measurements have been performed (fold axes orientations, small scale fracture measurements) and they have always been related to the corresponding stratigraphic unit.

Numerous calcite veins are observed in each outcrop. They permitted observation of fluid inclusions trapped in the crystals. Microthermometric measurements were performed to obtain homogenization temperatures that are considered to be representative of the trapping temperature conditions (Tilhac et al., 2013), thus giving an estimation of the temperature of the fluid that circulated. Double polished sections (~ 300 µm thick) of calcite crystals were prepared following Goldstein's (2003) recommendations. Homogenization temperature (Th) measurements were performed at the Laboratoire de Géologie de Lyon (LGL) on a Linkam THMS-600 heating-freezing stage connected to a programmable thermal control unit. Pure CO_2 fluid inclusions in quartz from Camperio, Central Alps (Poty and Stalder, 1974; Mullis et al., 1994) were used for calibration at CO_2 triple point (-56.6°C) and clathrate fusion (10.0°C) temperatures, and synthetic pure H_2O fluid inclusion in quartz for calibration of H_2O triple point (0.2°C) and critical point (375.13°C) temperatures. The accuracy of the measurements is estimated to be ± 1.0°C. Homogenization occurred in the liquid phase.

3. Results

3.1 Late Miocene tectono-sedimentary evolution of the NE of Ibiza Island.

Miocene-Pliocene units outcropping on the NE part of the Ibiza Island (Figs 1 & 2) were studied to establish their sedimentological and stratigraphic characteristics, to propose a tectono-sedimentary evolution and try to link them with the MSC event. The late Miocene (Fig. 4) is firstly composed (Unit 1), from base to top, of fossil-rich limestones (benthic foraminifera, corals, rhodoliths) accumulated in shallow marine environments. This sedimentary Unit presents some similarities with the Heterozoan unit previously described in Sorbas and therefore could be late Tortonian to lower Messinian in age (Bourrillot et al., 2010). In Portinatx area, it lies over the Mesozoic series. Some soft-sediment deformation structures have been observed at the top of Unit 1 at Punta Xarraca, where sandy to pebble rich clastic sediments have been injected to form clastic dykes in Unit 1 laminated limestones. Such soft-sediment deformation has been recognized as being triggered by earthquakes (Moretti and Sabato, 2007).

A detrital unit (Unit 2) formed by gravitational and fluvial processes in the nearshore environment overlays Unit 1. The edification of the coastal alluvial fans has been controlled by extensional faults that delimit the late Miocene distribution in the north-eastern Ibiza Island (Fig. 2).

Oolite, microbialite (thrombolite, stromatolite) -rich limestones (Unit 3) locally affected by ductile deformation onlap Unit 2. Usually, oolitic grainstones with herringbone structures and trough cross-stratifications are attributed to the lower part of Unit 3 (Unit 3-1) while microbialites dominate limestone

composition in the upper part (Unit 3-2). Unit 3 is interpreted as the TCC (Terminal Carbonate Complex) that is well known elsewhere in onland Spain (Bourillot et al., 2010; Clauzon et al., 2015). These three units were deposited in shallow water or nearshore environment. Locally, the TCC is covered by paleosols, wind dunes and mud/debris flows recording an onland deposition. A strong erosion of the Miocene and Mesozoic underlying series occurred after the deposition of the TCC. The important erosion and karstification surface locally shapes the valleys building the "calas" (local name for long and narrow gulfs) that reflect the present-day landscape (Fig. 3). This erosion and associated gravity flows are interpreted as evidence of emersion of the series (Lezin et al., 2017).

The erosion surface is filled with shallow marine calcarenites with gastropods, benthic foraminifera, and red algae that constitutes Unit 4 lying unconformably on Unit 3. It is attributed to the Zanclean Stage (early Pliocene) (Lezin et al., 2017). Aeolian bioclastic sands dated from Pleistocene (Del Valle et al., 2016) cover these deposits. Together with emersion evidence, we can undoubtedly relate the erosional surface between Unit 3 and Unit 4 to the MSC relative sea-level fall, the MES.

3.2. Folds and other deformational structures of the Mio-Pliocene series of Ibiza

Around Portinatx (Fig. 3) along Aigua Blanca cliff, a large succession of gentle folds can be observed in Unit 3 (Fig. 5). They have been recognized as synsedimentary structures (Simó Marfa, 1982) though not studied nor explained. Our measurements of the fold axes orientations permitted to group them in two main trends: 065°N and 140°N (Fig. 3). Due to the low eastward plunge of the series, the lower, middle and upper parts of the series are successively exposed from west to east. They correspond respectively to the western, the "Moscarter lighthouse" and the eastern areas presented below.

3.2.1. The western area

On Punta Galera Island, the exposed series are composed of limestones Unit 1 top, white clay Unit 2 and limestones Unit 3 (Fig. 6). The series is folded into a large and open syncline trending N 175° and resting on flat-lying Unit 1. In between, the argillaceous part of Unit 2 forms a wedge thickening toward the west. On the west side of the syncline, at the base of Unit 3, numerous soft-sediment deformation structures were observed. On vertical sections (Fig. 7a and b), they look like load structures with balls of grain rocks sinking into the argillaceous sediments of Unit 2. Whereas classical load structures show usually a regular and circular morphology (Moretti and Sabato, 2007), the structures of Punta Galera are linear like long ripples (Fig.7). The long axis of each load structure is orientated to the north, parallel to the syncline axis, suggesting the

development of the soft-sediment deformation structures during folding. Few metres above (Fig. 6c), calcite geodes, lined up at the bed top and wrapped in reworked carbonate sediments, indicate the occurrence of fluid circulation in the lower part of Unit 3.

In Cala Fondo area (Fig. 8) the exposed series shows the flat top of Unit 1 made of limestones, a reduced part of Unit 2 composed of white clay and topped by a strongly brecciated and partly recrystallized (neomorphism) limestone bed that can be attributed to the base of Unit 3. The outcrop outlines a large and open fold, trending N 25°, formed in the brecciated limestones and marls (Unit 2 and 3). Unit 2 marls are only a few metres thick near the syncline axis but they are thicker on both the western and eastern edges of the opened syncline. Some beds of black highly diagenetized limestones (recrystallization) are broken by small-scale fractures filled with red clays and that are trending either in the N-S or in the E-W directions.

3.2.2. The Moscarter lighthouse area

One of the most spectacular folded structure is exposed along the cliff, immediately east of the Moscarter lighthouse (Fig. 9). At that place, only Unit 3 is exposed, its base being under the present sea level. The calcareous herringbone beds form large rectangular blocks, about 100 m wide and approximately 15 m thick. The blocks appear to be little deformed but only moved apart like stretched rectangular boudins (Wegmann, 1932). Between the blocks, the laminated upper layers of Unit 3 are continuous and form scar folds made of a tight syncline between two open half anticlines (Hobbs et al., 1976; Goscombe et al., 2004). From their horizontal position over the blocks, the layers are laterally curved to a steep position between the block corners where limbs have been tilted up to 60° (Fig. 9). The tight synclines between blocks have developed in the laminated layers of Unit 3. In numerous places, these laminated layers have been totally transformed by diagenesis, resulting in the development of mm-scale calcite crystals (Fig. 10). In these specific areas of recrystallized layers, small fractures are formed perpendicular to bedding and are filled with red argillaceous sediments (Fig. 9c). These fractures develop close to tight syncline and are orientated from N 125° to N 145°, parallel to the fold axis. The laminated layers (Unit 3.1) and the oolitic grainstones are partially affected by diagenetic transformations. Transformations intensity increases towards the syncline axis. Simó-Marfa (1982) observed and described these transformations in the field and under the microscope. In the field, in the first stage of transformation, the color of the limestones is little affected but the sedimentary structures and the components are not visible and pores are filled with large crystals of calcite (Fig. 10 d-e). At an advanced stage, the limestones acquire a greyish color and a massive appearance. Black colored large crystals (1 to 3 cm) mark the

extreme case. Under the microscope, we observe in the first case a neomorphic reorganization allowing recognizing some grains. In both the advanced and extreme stages, a large amount of poecilitic cement destroys grains and sedimentary structures.

West of Moscarter lighthouse (Fig. 3), the large structure of the west Moscarter syncline (Fig. 11a) shows that the laminated layers (Unit 3-2), above the herringbone beds (Unit 3-1), are folded into two half anticlines with horizontal axes orientated N136° and N020° for the western and eastern folds respectively. Because of limited accessibility, the tight syncline between the two half anticlines cannot be precisely described. If the tight syncline can link the two non-parallel anticlines, it is probably not a cylindrical fold. Over the laminated beds, the bending of the layers progressively reduces upwards with the progressive onlap of paleosol layers that fill the depression (Fig. 11b). These paleosols are composed of reworked marls and are probably late Miocene in age (Lezin et al., 2017). The deformation is high on the limbs of the west Moscarter syncline (Fig. 11), where extensional deformation can be recognized from pinch and swell structures that have deformed both the laminated layers and the clastic sediments injected from the top into the layers. The extensional brittle deformation of the clastic sediments has formed small-scale normal faults with a stretching direction parallel to the layers (Fig. 11d). Some secondary folds, as shown in Figure 11c, have been estimated to have approximately N105° axis directions.

In the Aigua Blanca area (Figs. 5 and 12), the laminated layers are bent around the corners of the boudins; the lower layers being highly tilted. As a result, space is opened between the layers and filled with calcite wedges. The vertical orientation of the crystals shows that they have not grown in a completely open geodic volume but that they have progressively grown vertically in the space opened between the layers (Fig. 12).

In some places, such as over the bowl syncline located east of Portinatx, red clays filling numerous fractures or sedimentary dykes inject the upper layers (Fig. 12, area located on Figs. 3 & 5). The different intersections of the dykes are perpendicular or oblique but not any prevailing extensional direction has been recorded even after top view survey from a drone.

3.2.3. The eastern area

Punta des Gat is close to the distal part of the Cala d'en Serra section (Figs. 3 and 13) where the thickness of Unit 2 is highly reduced due to its facies variations from thick-bedded coarse conglomeratic deposits to the south (nearshore deposits) to thinner white clay deposits to the north (offshore deposits). Accordingly, sections in the Punta des Gat area display mainly the flat upper part of Unit 1 and some deformed

and strongly stretched layers of Unit 3 (Fig. 13). Coral rich carbonate Unit 1 shows evidence of neomorphism (recrystallization) and dissolution. Unit 3 is marked by the local presence of dissolution breccias and mineral floors. Both units are separated by some strongly deformed layers composed of mixed white and green clays, black recrystallized limestones, reddish limestones blocks, fragmented limestones separated by red clays (Fig. 14). The fractures range in strike from N 162° to N 050° but most of them are approximately N-S. Some of the clays may have a decalcification origin and the limestones correspond to the deformed and highly stretched part of Unit 3. On top of these deformed areas, lenses of Unit 4 material have been deposited. They are up to 10 m thick and they have been locally dated to the Zanclean Stage from microfaunal assemblages (Lezin et al., 2017).

In some places from the Punta des Gat area, clastic dykes and numerous veins filled with calcite crystals are observed within Unit 3. The veins, up to 20 cm thick, are always parallel to the layers and are filled with vertical calcite crystals. They are very similar to the calcite wedges observed west of the Moscarter lighthouse (Fig. 12). Fluid inclusions trapped in calcite have been observed in veins at different outcrops. Petrographic study shows that these inclusions are primary inclusions trapped during crystallization of calcite and growing of the veins. They present aqueous liquid and vapor phases at room temperature with a homogenous liquid/vapor ratio indicating the trapping of a single-phase aqueous fluid at trapping conditions. It was not possible to determine salinity of the fluid because inclusions are too small and calcite not transparent enough. Homogenization temperatures of the fluid inclusions could be measured. Only samples coming from the Cala de Ponent give clear results (Table 1). They indicate calcite crystallization between 190 and 260°C, relatively hot temperature for minerals formed under a relatively thin sedimentary cover. It is an indication of hot fluids circulation that can facilitate ductile deformation. In the Punta des Gat area, the three Miocene sedimentary units are very deformed under various processes from early diagenetic conditions to hot fluid ductile mechanisms. Unit 4 is not affected by these processes, either the deformation or the calcite veins formation.

4. Interpretation

4.1. A synthetic model of large-scale boudinage

From field observations, the structures of the Mio-Pliocene series of Ibiza appear to be organized in three areas. In the western area, folds involve the lower part of the series: they are narrow anticlines between larger opened synclines (Figs 6 and 8). Soft-sediment deformation observed at Punta Galera is an indication that folding started as soon as the deposit had occurred (Fig. 7). In the Moscarter area, only the mid and upper parts of the series can be observed, Unit 3-1 and Unit 3-2 respectively. The Unit 3-1 is mainly broken into large

blocks. The folds that develop in Unit 3-2 are narrow synclines between larger half anticlines. In the fold limbs, extensional deformation is observed from small scale normal faults (Fig. 11d) or tensile fractures formed under mode 1 opening conditions (Fig. 9c). Compressional structures have never been observed on the folds; it is an indication that there is not any neutral surface in the mid part of the folded layers and that folds have formed by bending instead of buckling (Fossen, 2010). In the Moscarter area, the bending of the laminated layers occurred during the progressive sedimentation of the paleosol layers (Fig. 11) and it stopped by the time of deposition of the upper carbonate. In the eastern area, the series has been highly stretched (Fig. 13): series thickness has been strongly reduced and some depressions have formed at the surface of the Miocene series. Marine and/or aeolian continental post-MSC sediments filled many of these depressions (Unit 4, Fig. 13b).

We propose that the late Miocene series of NE Ibiza (mainly Units 2 and 3) underwent extensional deformation. The thick homogeneous limestone bed with herringbones structures (Unit 3-1) is segmented into large scale symmetrical rectangular "torn boudins" (classification from Goscombe et al., 2004). The axes of the scar folds (Hobbs et al., 1976) formed in the inter-boudin (Fig. 15) indicate the extensional directions (Fig. 3). In analogue experiments of multidirectional extension (Victor and Moretti, 2006; Zulauf et al., 2011), the fractures formed between the blocks exhibit a large range of orientations but formation of true "chocolate tablet" patterns (Wegman, 1932; Ramsay, 1967) is not possible during one single phase of pure flattening strain (Zulauf et al., 2011) but requires two successive boudinage events (Goscombe et al., 2004). Unfortunately, there is a small number of boudins to be observed and few data are available. Nevertheless, the importance of both the 65°N and 140°N directions of folds (Fig. 3) suggests that extension occurred along roughly two perpendicular directions, forming badly organized "chocolate tablet" patterns. Large translational slides that have been described by Huntoon (1982), Huvenne et al. (2002) and Callot et al. (2008) could provide an illustration of large scale sliding and boudins (Fig. 15) that developed through the inhomogeneous deformation of the different layers during extension (Wegmann, 1932).

We propose a ductile stretching conceptual model of the Miocene series of north Ibiza (Fig. 16). The low tilting of the series to the east allows an exposition of the base of the boudins to the west, while the upper part is exposed to the east. Three types of boudinage deformation are observed, depending on their location within the sliding system:

1) On the western side of the studied area, rectangular boudins have been formed in Unit 3 (about 20 m-thick grainstone bed). During sliding and stretching, the mid part of the boudins sags gently to form the large syncline observed in Figure 6, while soft clay-rich Unit 2 escapes on the sides of the boudins where domes of

Unit 2 are observed. Some recrystallized limestones have been observed locally in Cala Fondo (Fig. 8) while in Punta Galera there are indications of soft-sediment deformation (Fig. 7).

2) Around the Moscarter lighthouse (Fig. 5), the grainstone layers of Unit 3 have been segmented to form large boudins while the laminated layers have bent to form ductile folds (Figs. 9 to 12). Diagenetic recrystallization of limestones occurred and large calcite veins formed between the bent layers. To the top, over the synclines that developed between the boudins, depressions have been formed and progressively filled with paleosols onlapping the laminated layers. In some places, subaerial erosion is observed. At the final stage, Unit 4 sediments have completed the infill of most of these depressions.

3) On the eastern side of the studied area, both Unit 2 and Unit 3 are stretched (Punta des Gat area, Figs. 3 and 13). The grainstone beds with herringbones of Unit 3 have formed irregular pinch and swell structures. Limestone recrystallization is observed everywhere at the base of stretched Unit 3 and calcite veins are numerous between the layers. It corresponds therefore to the most stretched domain of the studied area.

4. 2. Rheological control of soft layers over collapse structures

Rectangular boudins are recognized to have form under brittle conditions (Wegmann, 1932; Strömgård, 1973); a strong layer being segmented in relation to the ductile adjacent rocks while an increase of ductility leads to the formation of fishmouth boudins. In the Miocene series of NE Ibiza, the grainstones beds with herringbones have low fracture density and form large boudins (about 30 m thick and ca. 100 m wide). This dependence of fracture density on the textural parameter in carbonate rocks has been established by Ladeira and Price (1981), Hanks et al. (1997), Eyssautier-Chuine et al. (2002), Lezin et al. (2009), showing that the fracture density decreases when the grain content increases. The length to thickness ratio of the boudins (L/W according to Goscombe et al., 2004 classification) ranges from 2 to 4 in most natural examples. This closely fits the observations made in the Portinatx area but boudins appear to be larger in the WSW-ENE direction (L/W is up to 10) than in the NW-SE direction (Fig. 17).

Above and below the segmented competent bed, the incompetent layers deform under nearly ductile conditions with a low viscosity. Due to friction between the ductile layers and the boudins, most of the deformation is supposed to occur in between the boudins (Ramberg, 1955) and around the corners of the rectangular boudins where stress concentration is expected (Strömgård, 1973; Lloyd and Ferguson, 1981). Field observations of the NE Ibiza Miocene series agree with this theory. The high value of the L/W ratio is an indication of a high viscosity contrast between the boudins and the surrounding matrix because, in sedimentary

rocks, fracture spacing increases when the thickness of the incompetent layers increases or when its viscosity decreases (Ladeira and Price, 1981; Ji et al., 1998; Bai and Pollard, 2000). Deformation concentration in the block corners is observed in Figures 9 and 11. Calcite wedges indicating an important fluid circulation often mark it. Both a ductile layer and a high pore fluid pressure are the required conditions for sliding on a basal surface (Locat and Lee, 2002; Bryn et al., 2005), here the clay-rich distal part of Unit 2.

5. Discussion

5. 1. Large-scale boudinage versus active deformation

The studied deformation in the late Miocene series of northeastern Ibiza is fundamentally after the main compressional event of the Betic orogenesis (Fontboté et al., 1990; Gelabert et al., 1992; Sàbat et al., 1997). Unit 1 of Punta Xarraca area has been affected by soft-sediment injections probably triggered by earthquakes at the time of deposition or a short while later when Unit 2 deposition seems to be associated with the formation of large normal faults, probably during the extensional Serravalian-Tortonian phase. However, recent active deformation is recorded offshore in the surrounding areas and the Alicante shelf, and can be related to the general inversion of the Mediterranean domain (Gargani et al., 2010; Maillard and Mauffret, 2013; Gorini et al., 2015).

In some places, the occurrence of crossed fold directions could suggest the formation of superimposed folding with type 1 interference patterns, according to Ramsay's classification (1967). Nevertheless, both the occurrence of small-scale stretching deformation structures everywhere in the series and the formation of soft folds in the lower and upper layers of Unit 3, while the mid-layers remain fragmented but not folded, are indications of large scale ductile boudinage instead of classic superimposed folding.

Raft tectonic due to radial extension has been proposed from field analysis and from analogue experiments to accommodate large scale extension (Cobbold and Szatmari, 1991; Mauduit et al., 1997; Gaullier and Vendeville, 2005) but most of the models propose the formation of extensional tilted blocks over a mobile salt horizon. Such models cannot be exactly used to describe the structures formed in NE Ibiza where there is no evidence of tilted blocks neither any indication of a salt interval in the Miocene series. At the scale of the Ibiza outcrops, the geometry of the boudins is controlled by extensional fractures whereas shear fractures are formed during growth of raft systems on the extensional domain of a passive margin (Rouby et al., 2002).

5. 2. Indications of viscosity ratio

Torn boudins are formed by extension in materials with contrasted viscosities (Ramberg, 1955, Price and Cosgrove, 1990); the most rectangular boudins are observed in materials with the higher viscosity contrast (Lloyd and Ferguson, 1981). The transition from a rectangular boudin to a barrel-shape boudin is then an indication of the reduction of the strain rate and of the progression to a more ductile deformation (Goscombe et al., 2004). Over the west Moscarter syncline (Fig. 11), low strain rate conditions are indicated by the progressive deposition of marls (paleosol layers) during the deformation process, which could explain the softening of some boudin corners observed from various localities (Fig. 9). In the same way, the secondary folds, such as observed at the lower part of the east side of the Figure 11c, have been recognized by Lloyd and Ferguson (1981) as an early stage in the formation of barrel-shaped boudins.

The aspect ratio of the boudins (Fig. 17) is expressed by the L/W parameter (Fig. 15; Goscombe et al., 2004). As far as we can see, the L/W ratio seems to range from 2 to 4 in the NW-SE direction. The high value of the L/W ratio and the ductile deformation in the boudin corners could lead to opposite interpretations of the viscosity contrast but most examples from literature refer to metamorphic conditions while the Messinian series of NE Ibiza may have been deformed as synsedimentary structures (Simó Marfa, 1982). Ogata et al. (2014; 2016) have pointed out the interest of the analysis of soft-sediment deformation in comparison with metamorphic micro-tectonics (Passchier and Trouw, 1996). In the same way, the calcareous cross-laminated grainstones deform as elongated boudins bounded by the ductile laminated layers. The high L/W ratio is an indication that the boudins are separated by a few vertical fractures, as usually observed in grainstones. Nevertheless, the ductile behavior of boudin corners is an indication that the viscosity ratio between the boudins and the folded laminated layers was probably quite lower than what may be expected from the boudins shape. When only meter scale boudinage is recorded in the literature (Goscombe et al., 2004), the development of such large-scale boudinage (L>100m) might be a specificity of soft-sediment deformation in carbonate sedimentary rocks.

5. 3. Soft-sediment deformation helped by fluid circulations

Such large-scale sedimentary boudinage requires stretching and sliding of the sedimentary layers. Huvenne et al. (2002) described some large translational slides and their occurrence appears to be favored by elevated pore-pressure. The high level of limestone recrystallization and the numerous occurrences of calcite veins in Moscarter area are indications of high fluid pressure that can reduce the frictional resistance to sliding (Locat and Lee, 2002; Sultan et al., 2004; Alves, 2015) and weaken layers within stratified sequences (Masson et

al., 2006). Under these conditions, sliding can develop on slopes as low as 1° (Haflidason et al., 2004) and among the causal factors is the sea level drawdown (Hilbrecht, 1989; Spence and Tucker, 1997; Dreyer et al., 1999; Sultan et al., 2004; Callot et al., 2009). The early lithification of the carbonate layers compared to the soft-deformation of the detrital layers (Callot et al., 2008) can lead to stress reduction on the interface. All that produces an increase in boudins width (Marques et al., 2012) and easy sliding of Unit 3 carbonate layers on Unit 2 clastic layers.

Both the deposition of paleosols during the bending of Unit 3 and the formation of calcite wedges on the fold limbs are indications of a long time process during large fluid circulation. The high values of the fluid temperatures, up to 250°C, require a deep crustal origin of the fluids that can be explained by the immediate vicinity of the compressional and extensional structures of Ibiza Island (Etheve et al., 2016) with regard to the destabilization of the messinian carbonate platform.

5. 4. Submarine or subaerial sliding conditions and triggering conditions

On a Mediterranean scale, the MSC sea-level drawdown is responsible for a large transfer of sediment from shelves to basin where large clastic layers are observed (Bache et al., 2009; Madof et al., 2019). Cameselle and Urgeles (2017) have proposed that a large margin collapse in the Valencia basin was triggered by the sea-level drawdown during the MSC. Offshore, between Ibiza and Mallorca islands, the MSC-related unit displays 200 to 400m-long rafts cut by low-angle normal faults interpreted as thin-skinned deformation due to gliding on a detachment surface (Maillard et al., 2014). Because the seismic profiles do not reach the upper slope, it is difficult to correlate this margin collapse with our observations of large-scale boudinage on the upslope of Ibiza Island. Nevertheless, both appear to have been caused by the same major event of sea-level drawdown, which can be considered as long-term triggering (Sultan et al., 2004). It produced the translational sliding of soft carbonate layers of the late Miocene on a gentle slope; the layers already cemented by early diagenetic processes can break and slide while the softer layers are bent around the blocks.

The stretching deformation appears to increase to the NE of Portinatx but boudins are shorter in the NW-SE direction; all indicates that the sliding has developed mostly northward, towards the Valencia Basin. The sliding has occurred during the emersion of the MSC, as recorded by the onlap of paleosols over some Unit 3 folds. Finally, MSC erosion took place in the channels created by the synclines depressions and lowered areas (Figs. 13 and 16), as shown by their progressive filling by Unit 4 shallow marine deposits during the Zanclean reflooding (Gaullier et al., 2014; Giresse et al., 2015; Maillard et al., 2016).

420 It is difficult to infer the exact chronology between the MES, the gravity flows, and paleosols
421 expansion, but most are evidence of subaerial events produced after bending of Unit 3. Continental deposits like
422 fluvial systems were also evidenced onland in Spain, Morocco and Eastern Mediterranean regions, developing
423 during the peak of the MSC (Do Couto et al., 2014; Cornée et al., 2016, Madof et al., 2019). Bending of Unit 3
424 under soft conditions, could have begun while still underwater during the beginning of the drawdown, but more
425 probably in subaerial conditions. If such subaerial destabilization has been evidenced offshore, mostly on the
426 slopes during the MSC sea-level fall, examples on the shelf remain poorly documented, except where evaporites
427 are present in the pre-MSC peak succession (Sorbas: Clauzon et al. 2015; Bourrillot et al., 2010; Cyprus:
428 Orszag-Sperber et al., 2009). Mass flows are documented within fluvio-lacustrine Lago-Mare deposits in Crete,
429 interpreted as triggered by an early Pliocene tectonic event, though the slope failure is the MES (Zachariasse et
430 al., 2008; Alves and Lourenço, 2010). Note that in the eastern Mediterranean area, a change of tectonic regime
431 occurred just at the end of Miocene (Hall et al., 2005) and that thick-skin tectonics could be overprinted by thin-
432 skin salt tectonics, meaning that MSC (with sea-level drop and collapses) could be responsible for complex
433 deformation occurring precisely at the Messinian / Pliocene boundary (Maillard et al., 2010).
434

435 ## 7. Conclusions

436 Most of the deformation of the late Miocene series of north-western Ibiza Island appears as
437 synsedimentary large scale boudinage. The calcareous herringbone layers of Unit 3 (U3-1) form large
438 rectangular to barrel-shaped boudins. The overall geometry of these large blocks, reconstructed from mapping
439 and structural data, corresponds to a badly organized “chocolate tablet” model that likely reveals a
440 multidirectional extension. The increasing block deformation to the north suggests an increase of stretching, or
441 translational sliding, in that direction. It could have been favored by the north-eastward rapid increase in clay
442 content of Unit 2 at the base of boudins and by the large circulation of relatively hot fluids, up to 260°C.
443 Along and between Unit 3 boudins, the laminated layers (U3-2) form ductile scar folds. At the corners
444 and between the boudins, the progressive bending of these laminated layers of the upper part of Unit 3 manages
445 spaces filled with calcite crystal wedges that provide an indication for important fluid circulation during
446 deformation. Unit 3 recrystallization above, below and between the boudins strengthens the indication of large
447 fluid circulation supporting the conditions of ductile deformation.
448 The topographic depressions formed by the boudinage of the late Miocene series have controlled the
449 drainage patterns and the coeval development of erosive channels. In Ibiza Island, the occurrence of continental

debris flows within these channels testifies that deformation of soft sediments occurred in subaerial conditions, shortly after their deposition. The progressive infill of paleosols over some of the synsedimentary synclines confirms that the deformation developed relatively slowly but resulted in an important deformation during the emersion period. The process of margin collapse during Messinian sea-level drawdown, proposed elsewhere in the Mediterranean Basin, appears to be responsible for the translational sliding, boudinage and large-scale collapse of the late Miocene series on the northeastern Ibiza Margin.

Acknowledgments

The authors acknowledge the french "Action Marges" INSU program for the financial support of this project. The authors thank Stéphane Bonnet who kindly lent us a drone and Christiane Cavaré-Hester for her enthusiastic and effective help in the preparation of the line drawing of the figures. The paper has largely benefited from the constructive criticisms of Kei Ogata, Dominque Frizon de Lamotte, and three anonymous reviewers.

References

Acosta, J., Canals, M., Lopez-Martinez, J., Munoz, A., Herranz, P., Urgeles, R., Palomo, C., Casamor, J.L., 2002. The Balearic Promontory geomorphology (western Mediterranean): morphostructure and active processes. Geomorphology, 49, 177–204.

Acosta, J., Fontán, A., Muñoz, A., Muñoz-Martín A., Rivera, J., Uchupi, E. 2013. The morpho-tectonic setting of the Southeast margin of Iberia and the adjacent oceanic Algero-Balearic Basin. Mar. and Pet. Geol. 45, 17-41.

Alfaro, P., Delagado, J., Estevez, A., Soria J.M. and Yébenes, A., 2002. Onshore and offshore compressional tectonics in the eastern Betic Cordillera (SE Spain), Mar. Geol. 186, pp. 337–349.

Allen, J. R. L., 1982. Developments in Sedimentology, 30B. Sedimentary structures, their character and physical basis. Vol. II, chapter 9, Soft-sediment deformation structures. 343-393. Elsevier, 663p.

Alves, T. M., 2015. Submarine slide blocks and associated soft-sediment deformation in deep-water basins: A review. Marine and Petroleum Geology, 67, 262-285.

Alves, T. M., Lourenço, S. D. N., 2010. Geomorphologic features related to gravitational collapse: Submarine landsliding to lateral spreading on a Late Miocene-Quaternary slope (SE Crete, eastern Mediterranean. Geomorphology, 123, 13-33. Doi:10.1016/j.geomorph.2010.04.030.

Bache, F.; Olivet, JL.; Gorini, C.; Rabineau, M.; Baztan, J; Aslanian, D.; Suc, J.P., 2009. "Messinian Erosional and Salinity Crises: View from the Provence Basin (Gulf of Lions, Western Mediterranean)". Earth Planet. Sci. Lett. 286, 139-157.

Bai, T., Pollard, D., 2000. Fracture spacing in layered rocks: a new explanation based on the stress transition. Journal of Structural Geology, 22, 43-57.

Bourillot, R., Vennin, E., Rouchy, J.-M., Durlet, C., Rommevaux, V., Kolodka, C., Knap, F., 2010. Structure and evolution of a Messinian mixed carbonate-siliciclastic platform: the role of evaporates (Sorbas Basin, South-east Spain). Sedimentology, 57, 477-512.

Bryn, P., Berg, K., ForsbergC. F., Solheim A., Kvalstad, T. 2005. Explaining the Storegga slide. Marine and Petroleum Geology, 22, 11-19.

Callot, P., Sempere, T., Odonne, F., Robert, E., 2008. Giant submarine collapse of a carbonate platform at the Turonian-Coniacian transition: The Ayabacas Formation, southern Peru. Basin Research, **20**, 333-357.

Callot, P., Odonne, F., Debroas, E.-J., Maillard, A., Dhont, D., Basile, C., Hoareau, G., 2009. Three-dimensional architecture of submarine slide surfaces and associated soft-sediment deformation in the Lutetian Sobrarbe deltaic complex (Ainsa, Spanish Pyrenees). Sedimentology, 56, 1226-1249.

Cameselle, A., Urgeles, R., 2017. Large-scale margin collapse during Messinian early sea-level drawdown: the SW Valencia trough, NW Mediterranean. Basin Research, 29, 576-595.

Cardozo, N., Allmendinger, R.W., 2013. Spherical projections with OSXStereonet: Computers & Geosciences, v. 51, p. 193 – 205, doi:10.1016/j.cageo.2012.07.021.

C.I.E.S.M (2008) The Messinian salinity crisis from mega-deposits to microbiology. In: Briand, F. (Ed.), A consensus report, in 33eme CIESM Workshop Monographs, 33. CIESM, 16, bd de Suisse, MC-98000, Monaco, pp. 1–168.

Clauzon, G., Suc, J.-P., Gautier, F., Berger, A., Loutre, M.-F., 1996. Alternate interpretation of the Messinian salinity crisis: controversy resolved? Geology, 24, 363–366.

Clauzon, G., Suc, J.-P., Do Couto, D., Jouannic, G., Melinte-Dobrinescu, M. C., Jolivet, L., Quillévéré, F., Lebret, N., Mocochain, L., Popescu, S.-M., Martinell, J., Doménech, R., Rubino, J.-L., Gumiaux, C., Warny, S., Bellas, S. M., Gorini, C., Bache, F., Rabineau, M., Estrada, F., 2015. New insights on the Sorbas Basin (SE Spain): The onshore reference of the Messinian Salinity Crisis. Marine and Petroleum Geology, 66, 71-100.

Cobbold, P. R., Szatmari, P., 1991. Radial gravitational gliding on passive margins. Tectonophysics, 188, 249-289.

Cornée J.J., Münch, P., Achalhi, M., Merzeraud, G., Azdimousa, A., Quillévér, F., Melinte-Dobrinescu, M., Chaix, C., Ben Moussa, A., Lofi, J., Séranne, M., Pierre Moissette, P., 2016. The Messinian erosional surface and early Pliocene reflooding in the Alboran Sea: New insights from the Boudinar basin, Morocco. Sedimentary Geology 333, 115–129.

Del Valle, L., Gomez-Pujol, L., Fornos, J. J., Timar-Gabor, A., Anechiteie-Deacu, V., Pomar, F., 2016. Middle to Late Pleistocene dunefields in rocky coast settings at Cala Xuclar (Eivissa, Western Mediterranean): Recognition, architecture and luminescence chronology. Quaternary International, 407, 4-13.

Do Couto, D., Popescu, S.M., Suc, J.-P., Melinte-Dobrinescu, M.C., Barhoun, N., Gorini, C., Jolivet, L., Poort, J., Jouannic, G., Auxietre, J.-L., 2014. Lago Mare and the Messinian Salinity Crisis: evidence fromthe Alboran Sea (S. Spain). Marine and Petroleum Geology 52, 57–76.Dreyer, T., Corregidor, J., Arbues, P., Puigdefabregas, C., 1999. Architecture of the tectonically influenced Sobrarbe deltaic complex in the Ainsa Basin, northern Spain. Sedimentary Geology, 127, 127-169.

Dreyer T., Corregidor J., Arbues P., Puigdefabregas C., 1999. Architecture of the tectonically influenced Sobrarbe deltaic complex in the Ainsa Basin, northern Spain. Sedimentary Geology, 127, 127-169.

526 Driussi, O., Maillard, A., Ochoa, D., Lofi J., Chanier, F., Gaullier, V., Briais, A., Sage, F., Sierro, F., Garcia, M.,
527 2014. Messinian Salinity Crisis deposits widespread over the Balearic Promontory: Insights from new
528 high-resolution seismic data. Marine and Petroleum Geology, 66, 41-54.
529 Driussi O., Briais A., Maillard A., 2015. Evidence for transform motion along the South Balearic margin and
530 Implications for the kinematics of opening of the Algerian basin. Bull. Soc. Géol. France 186, 353-370.
531 Durand-Delga M., Freneix S., Magne J., Meon H., Rangheard Y., 1993. La série saumâtre et continentale d'âge
532 Miocène moyen et supérieur d'Eivissa (ex-Ibiza, Baléares). Acta Geol. Hisp. Barcelona, 28,33-46.
533 Ethève, N., Frizon De Lamotte, D., Mohn, G., Martos, R., Roca, E., Blanpied, C., 2016. Extensional vs
534 contractional Cenozoic deformation in Ibiza (Balearic Promontory, Spain): Integration in the West
535 Mediterranean back-arc setting. Tectonophysics, 682, 35–55.
536 Eyssautier-Chuine, S., Odonne, F., Massonnat, G., 2002. Control of bioclast abundance on natural joint density
537 in carbonate rocks: data from Oman, Provence and Languedoc (France). Terra Nova, 14, 198-204.
538 Fontbote, J.M., Guimera, J., Roca, E., Sabat, F., Santanach, P.N., Fernandez-Ortigosa, F., 1990. The Cenozoic
539 geodynamic evolution of the Valencia Trough (western Mediterranean). Rev. Soc. Geol. Esp., 3, 249–
540 259.
541 Fossen, H., 2010. Structural Geology. Cambridge University Press, 463p.
542 Fourcade, E., Chauve, P., Chabrier, G., 1982. Stratigraphie et tectonique de l'île d'Ibiza, témoin du prolongement
543 de la nappe subbétique aux Baléares (Espagne). Eclogae geol. Helv., 75 (2), 415–436.
544 Frizon de Lamotte D., Andrieux J., Guézou J.C., 1991. Cinématique des chevauchements néogènes dans l'arc
545 bético-rifain, discussions sur les modèles géodynamiques. Bull. Soc. géol. Fr., 162, 611-626.
546 Gargani, J., Rigollet, C., Scarselli, S., 2010. Isostatic response and geomorphological evolution of the Nile valley
547 during the Messinian salinity crisis. Bull. Soc. Géol. Fr., 181, 19-26.
548 Gaullier, V., Vendeville, B. C., 2005. Salt tectonics driven by sediment progradation: Part II-Radial spreading of
549 sedimentary lobes prograding above salt. AAPG Bulletin, 89, 1081-1089.
550 Gaullier V., Chanier F., Lymer G., Vendeville B., Maillard A., Thinon I., Lofi J., Sage F., Loncke L., 2014. Salt
551 tectonics and crustal tectonics along the Eastern Sardinian margin, Western Tyrrhenian : New insights
552 from the « METYSS 1 » cruise. Tectonophysics, 615-616 : 69-84.
553 Gautier, F., Clauzon, G., Suc, J.P., Cravatte, J., Violenti, D., 1994. Age et durée de la crise de salinité
554 messinienne. Compte Rendu de l'Académie des Sciences de Paris, 318 (2): 1103-1109.
555 Gelabert, B., Sàbat, F., Rodríguez-Perea, A., 1992. A structural outline of the Serra the Tramontana of Majorca
556 (Balearic Islands). Tectonophysics, 203, 167–183.
557 Gelabert, B., Sàbat, F., Hardy, S., Rodríguez-Perea, A., 2004. Significance of inherited normal faults during
558 inversion tectonics: an example from the Tramuntana Range, Mallorca. Geodinamica Acta, 17, 363-373.
559 Giresse P., Bassetti M.-A., Chanier F., Gaullier V., Maillard A., Thinon I., Lofi J., Lymer G., Reynaud J.-Y.,
560 Negri A., Saavedra M., 2015. Depositional environment and age of some key Late Pliocene to Early
561 Quaternary deposits on the underfilled Cedrino paleovalley (Orosei) : Insight into the Neogene
562 geodynamic evolution of Sardinia. Quaternary International, 357, 220-236.
563 Goldstein, R.H., 2003. Petrographic analysis of fluid inclusions. In: Samson, I., Anderson, A., Marshall, D.
564 (Eds.), Fluid inclusions: Analysis and Interpretation. Mineral. Assoc. Can., Short Course Ser., 32, pp. 9-
565 53.

566 Gorini C., Montadert L., Rabineau M., 2015. New imaging of the salinity crisis : Dual Messinian lowstand
567 megasequences recorded in the deep basin of both the eastern and western Mediterranean. Marine and
568 Petroleum Geology, 66, 278-294.
569 Goscombe, B. D., Passchier, C. W., Hand, M., 2004. Boudinage classification: end-member boudin types and
570 modified boudin structures. J. Struct. Geol., 26, 739-763.
571 Haflidason, H., Sejrup, H. P., Nygård, A., Mienert, J., Bryn, P., Lien, R., Forsberg, C. F., Berg, K., Masson, D.,
572 2004. The Storegga Slide: architecture, geometry and slide development. Marine Geology, 213, 201-234.
573 Hall, J., Aksu, A.E., Calon, T.J. & YaSar, D., 2005. Varying tectonic control on basin development at an active
574 microplate margin: Latakia Basin, Eastern Mediterranean. Mar. Geol., 221, 15-60.
575 Hanks, C. L., Lorenz, J. C., Teufel, L., Krumhardt, A. P., 1997. Lithologic and structural controls on natural
576 fracture distribution and behavior within the Lisburne group, Northeastern Brooks range and north slope
577 subsurface, Alaska. AAPG Bulletin, 81, 1700-1720.
578 Hilbrecht, H., 1989. Redeposition of late Cretaceous pelagic sediments controlled by sea-level fluctuations.
579 Geology, 17, 1072-1075.
580 Hobbs, B. E., Means, W. D., Williams, P. F., 1976. An Outline of Structural Geology. Wiley int. ed., 571p.
581 Hsü, K. J., Ryan, W. B. F., Cita M. B., 1973. Late Miocene Desiccation of the Mediterranean. Nature, 242, 240–
582 244.
583 Huntoon, P. W., 1982. The Meander anticline, Canyonlands, Utah: An unloading structure resulting from
584 horizontal gliding on salt. Geo. Soc. Am. Bull., 93, 941-950.
585 Huvenne, V. A. I., Croker, P. F., Henriet, J.-P., 2002. A refreshing 3D view of an ancient sediment collapse and
586 slope failure. Terra Nova, 14, 33-40.
587 Ji, S., Zhu, Z., Wang, Z., 1998. Relationship between joint spacing and bed thickness in sedimentary rocks:
588 effects of interbed slip. Geo. Mag., 135, 637-655.
589 Krijgsman, W., Hilgen, F., Raffi, I., Sierro, F., Wilson, D., 1999. Chronology, causes and progression of the
590 Messinian salinity crisis. Nature, 400, 652–655.
591 Ladeira, F. L., Price, N. J., 1981. Relationship between fracture spacing and bed thickness. J. Struct. Geol., 3,
592 179-183.
593 Lastras G., Canals M., Urgeles R., Hughes-Clarke J.E., Aacosta J., 2004. Shallow slides and pockmark swarms
594 in the Eivissa channel, western Mediterranean sea. – Sedimentology, 51, 837-850.
595 Leeder M., 1987. Sediment deformation structures and the palaeotectonic analysis of sedimentary basins, with a
596 case study from the Carboniferous of northern England. In: “Deformation of Sediments and Sedimentary
597 Rocks” M. E. Jones & R. M. F. Preston eds. Geol. Soc. London, Spec. Pub., 29, 137-146.
598 Lezin, C., Odonne, F., Massonnat, G. J., Escadeillas, G., 2009. Dependence of joint spacing on rock properties in
599 carbonate strata. AAPG Bulletin, 93, 271-290.
600 Lezin, C., Driussi, O., Bourillot, R., Maillard, A., Chanier, F., Odonne, F., 2014. Le Miocène terminal de l’île
601 d’Ibiza : étude des dépôts liés à la crise messinienne. Poster. 24ème Réunion des Sciences de la Terre
602 (RST). Pau. 27-31 octobre.
603 Lézin C., Maillard A., Odonne F., Colinet G., Chanier F., Gaullier V., 2017. Tectono-sedimentary evolution of
604 the Miocene-Pliocene series of Ibiza: new onshore evidence of the Messinian Salinity Crisis (MSC) IMS
605 Toulouse oct. 2017, Poster.

606 Lloyd, G. E., Ferguson, C. C., 1981. Boudinage structure: some new interpretations based on elastic-plastic finite
607 element simulations. J. Struct. Geol., 3, 117-128.
608 Locat, J., Lee, H. J., 2002. Submarine landslides: advances and challenges. Can. Geotech. J., 39, 193-212.
609 Lofi, J., Deverchere, J., Gaullier, V., Gillet, H., Guennoc, P., Gorini, C., Loncke, L., Maillard, A., Sage, F.,
610 Thinon, I., 2011. Seismic Atlas of the "Messinian Salinity Crisis" Markers in the Mediterranean and
611 Black Seas. Geological French Society, World Geological Map Commission, Paris, France. 72 pp.
612 Lowe, D. R., 1975. Water escape structures in coarse grained sediments. Sedimentology, 22, 157-204.
613 Madof, A. S., Bertoni, C., Lofi, J., 2019. Discovery of vast fluvial deposits provides evidence for drawdown
614 during the late Miocene Messinian salinity crisis. Geology, 47, 171-174.
615 Maillard, A., Mauffret, A., Watts, A.B., Torne, M., Pascal, G., Buhl, P., Pinet, B., 1992. Tertiary sedimentary
616 History and structure of the Valencia Trough (Western Mediterranean). Tectonophysics, 203, 57–76.
617 Maillard, A., Huebscher, C., Benkhelil, J., Tahchi, E., 2010. Messinian markers in the Cyprus Arc: tectonics or
618 Messinian Salinity Crisis erosion indicators? Basin Research 23, 146–170.
619 Maillard, A., Mauffret, A., 2013. Structure and present-day compression in the offshore area between Alicante
620 and Ibiza Island (Eastern Iberian Margin). Tectonophysics, 591, 116-130.
621 Maillard, A., Driussi, O., Lofi, J., Briais, A., Chanier, F., Hübscher, C., Gaullier, V., 2014. A complete record of
622 the Messinian markers in the SW Mallorca area (Balearic Promontory, Spain). Marine Geol 357, 304-
623 302.
624 Maillard A., Lezin C., Odonne F., Chanier F., Gaullier, V., 2016. Messinian Erosion Surface onshore/offshore
625 Ibiza Island, Balearic Promontory. COST-ANR MEDSALT Symposium, University of PALERMO 24-26
626 October2016.
627 Maltman, A., 1984. On the term "soft-sediment" deformation. Journal of Structural Geology, 6, 589-592.
628 Marques, F. O., Fonseca, P. D., Lechmann, S., Burg, J.-P., Marques, A. S., Andrade, A. J. M., Alves, C., 2012.
629 Boudinage in nature and experiment. Tectonophysics, 526-529, 88-96.
630 Masson, D. G., Harbitz, C. B., Wynn, R. B., Pedersen, G., Løvholt, F., 2006. Submarine landslides: processes,
631 triggers and hazard prediction. Phil. Trans. R. Soc. A, 364, 2009-2039.
632 Mauduit, T., Guerin, G., Brun, J.-P., Lecanu, H., 1997. Raft tectonics: the effects of basal slope angle and
633 sedimentation rate on progressive extension. J. Struct. Geol., 19, 1219-1230.
634 Mauffret, A., Maillard, A., Pascal, G., Torne, M., Buhl, P., Pinet, B., 1992. Long-listening Multichannel
635 Seismic Profiles in the Valencia Trough (Valsis 2) and the Gulf of Lions (ECORS): a comparison. In:
636 Banda, E., Santanach, P. (Eds.), Geology and Geophysics of the Valencia Trough, Western
637 Mediterranean: Tectonophysics, 203, 285–304.
638 Mauffret, A., Durand de Grossouvre, B., Tadeu Dos Reis, A., Gorini, C., Nercessian, A., 2001. Structural
639 geometry in the eastern Pyrenees and western Gulf of Lion (Western Mediterranean). Journal of
640 Structural Geology, 23, 1701 – 1726.
641 Moretti, M., Sabato, L., 2007. Recognition of trigger mechanisms for soft-sediment deformation in the
642 Pleistocene lacustrine deposits of the Sant'Arcangelo Basin (Southern Italy): Seismic shock vs.
643 overloading. Sedimentary Geology, 196, 31-45.

644 Mullis, J., Dubessy, J., Poty, B., O'Neil, J., 1994. Fluid regimes during late stages of a continental collision:
645 physical, chemical and stable isotope measurements of fluid inclusions in fissure quartz from a
646 geotraverse through the Central Alps, Switzerland. Geochemica et Cosmochimica Acta 58, 2239-2267.
647 Ogata, K., Pogačnik, Ž., Pini, G. A., Tunis, G., Festa, A., Camerlenghi, A., Rebesco, M., 2014. The carbonate
648 mass transport deposits of the Paleogene Friuli Basin (Italy/Slovenia): Internal anatomy and inferred
649 genetic processes. Marine Geology, 356, 88-110.
650 Ogata, K., Pini, G. A., Festa, A., Pogačnik, Ž., Lucente, C. C., 2016. Meso-scale kinematic indicators in
651 exhumed mass transport deposits: definitions and implications. In: Submarine Mass Movement and their
652 Consequences, G. Lamarche, J. Mountjoy, S. Bull, T. Hubble, S. Krastel, E. Lane, A. Micallef, L.
653 Moscardelli, C. Mueller, I. Pecher & S. Woelz (eds). Advances in Natural and Technological Hazards
654 Research. Springer, 41,461-468.
655 Orszag-Sperber, F., Caruso, A., Blanc-Valleron, M.M., Merle, D., Rouchy, J.M., 2009. The onset of the
656 Messinian salinity crisis: insights from Cyprus sections. Sediment. Geol., 217, 52-64.
657 Owen, G., 1987. Deformation processes in unconsolidated sands. Deformation of Sediments and Sedimentary
658 Rocks; Jones M. E. & Preston R. M. F. (eds). Geol. Soc. of London, Spec. Pub., 29, 11-24.
659 Passchier, C. W., Trouw, R. A. J., 1996. Micro-tectonics. Springer, 289 p.
660 Platt, J. P., Whitehouse, M. J., Kelley, S. P., Carter, A., Hollick, L., 2003. Simultaneous extensional exhumation
661 across the Alboran Basin: Implications for the causes of late orogenic extension, Geology, 31(3), 251-
662 254.
663 Platt, J.P., Behr, W.M., Johanesen, K.,Williams, J.R., 2013. The Betic–Rif arc and its orogenic hinterland: a
664 review. Annu. Rev. Earth Planet. Sci. 41, 313–357.
665 Price, N. J., Cosgrove, J. W., 1990. Analysis of Geological Structures. Cambridge Univ. Press. 502p.
666 Poty, B., Stalder, H.A., 1974. Fluid inclusions studies in quartz from fissures of Western and Central Alps.
667 Schweizerische Mineralogische und Petrographische Mitteilungen 54, 717-752.
668 Ramberg, H., 1955. Natural and experimental boudinage and pinch-and-swell structures. The Journal of
669 Geology, 63, 512-526.
670 Ramos Guerrero, E., Rodriguez-Perea, A., Sabat, F., Serra-Kiel, J., 1989. Cenozoic tectonosedimentary
671 evolution of Mallorca Island. Geodin. Acta, 3, 53–72.
672 Ramsay, J. G., 1967. Folding and Fracturing of Rocks. Mc Graw Hill. 568 p.
673 Rangheard, Y., 1971. Étude géologique des îles d'Ibiza et de Formentera (Baléares). Mem. Inst. Geol. Min.
674 Espana. 82, 340 p.
675 Rangheard, Y., Müller, C., Durand-Delga, M., 2011. Apport de la micropaléontologie, spécialement du
676 nannoplancton, à la connaissance de l'évolution géologique au Miocène de l'île d'Eivissa (Ibiza,
677 Baléares, Espagne). Contribution of micropaleontology (especially nannofossils) to reconstruct the
678 Miocene geological evolution of the island of Eivissa (Ibiza, Balearic Islands, Spain). C. R. Palevol, **10**,
679 537–549.
680 Roca, E., 2001. The Northwest-Mediterranean basin (Valencia Trough, Gulf of Lions and Liguro-Provencal
681 basins): structure and geodynamic evolution. In: Ziegler, P.A., Cavazza, W., Robertson, A.F.H. (Eds.),
682 Peri-TethysMemoir, IGCP 369: Peri Tethyan Rift/Wrench Basins and Passive Margins. Mem. Mus. Natl.
683 Hist. Nat., Paris, pp. 671–706.

Roca E., Guimera, J., 1992. The Neogene structure of the Eastern Iberian margin: structural constraints on the crustal evolution of the Valencia Trough (Western mediterranean). Tectonophysics 203, 203-218.

Rouby, D., Raillard, S., Guillocheau, F., Bouroullec, R., Nalpas, T., 2002. Kinematics of a growth fault/raft system on the West African margin using 3-D restoration. Journal of Structural Geology, 24, 783-796.

Rouchy, J.M., Caruso, A., 2006. The Messinian salinity crisis in the Mediterranean basin: A reassessment of the data and an integrated scenario. Sedimentary Geology, 188-189, 35-67.

Roveri, M., Flecker, R., Krijgsman, W., Lofi, J., Lugli, S., Manzi, V., Sierro, F.J., Bertini, A., Camerlenghi, A., De Lange, G., 2014. The Messinian Salinity Crisis: past and future of a great challenge for marine sciences. Marine Geology, 352, 25–58.

Ryan, W.B.F., 2008. Modeling the magnitude and timing of evaporative drawdown during the Messinian salinity crisis. – Stratigraphy, 5, 1, 227- 243.

Sàbat, F., Roca, E., Muñoz, J.A., Vergés, J., Santanach, P., Sans, M., Masana, E., Estévez, A., Santisteban, C., 1997. Role of extension and compression in the evolution of the eastern margin of Iberia: the ESCI-Valencia Trough seismic profile. Rev. Soc. Geol. España, 8, 431–448.

Sàbat, F., Gelabert, B., Rodriguez-Perea, A., Giménez, J., 2011. Geological structure and evolution of Majorca: Implications for the origin of the Western Mediterranean. Tectonophysics, 510, 217-238.

Sanz De Galdeano, C., 1990. Geologic evolution of the Betic Cordilleras in the Western Mediterranean, Miocene to the present. Tectonophysics, 172, 107–119.

Simo Marfa, J. A., 1982. El Mioceno terminal de Ibiza y Formentera. Thesis Universidad de Barcelona, 197 p.

Spence, G. H., Tucker, M. E., 1997. Genesis of limestone megabreccias and their significance in carbonate sequence stratigraphic models: a review. Sed. Geol., 112, 163-193.

Strömgård, K. E., 1973. Stress distribution during formation of boudinage and pressure shadows. Tectonophysics, 16, 215-248.

Sultan, N., Cochonat, P., Canals, M., Cattaneo, A., Dennielou, B., Haflidason, H., Laberg, J. S., Long, D., Mienert, J., Trincardi, F., Urgeles, R., Vorren, T. O., Wilson, C., 2004. Triggering mechanisms of slope instability processes and sediment failures on continental margins: a geotechnical approach. Marine Geology, 213, 291-321.

Tilhac, R., Guillaume, D., Odonne, F., 2013. Fluid circulation and deformational gradient in north-Pyrenean flyschs : Example from the Saint-Jean-de-Luz basin (France). Tectonophysics, 608, 832_846.

Victor, P., Moretti, I., 2006. Polygonal fault systems and channel boudinage: 3D analysis of multidirectional extension in analogue sandbox experiments. Marine and Petroleum Geology, 23, 777-789.

Wegman, C. E., 1932. Note sur le boudinage. Bulletin de la Société Géologique de France, 2, 477-491.

Zachariasse, W. J., Van Hinsbergen, D. J. J., Fortuin, A. R., 2008. Mass wasting and uplift on Crete and Karpathos during the early Pliocene related to initiation of south Aegean left-lateral, strike-slip tectonics. GSA Bulletin, 120, 976-993. Doi: 10.1130/B26175.1.

Zulauf, J., Zulauf, G., Kraus, R., Gutierrez-Alonso, G., Zanella, F., 2011. The origin of tablet boudinage: Results from experiments using power-law rock analogs. Tectonophysics, 510**,** 327-336.

724 # Figure captions

725

726 Figure 1. Location map of Ibiza and Balearic islands, south-east of Iberia. The Balearic Promontory is located
727 between extensional basins that opened during early Miocene: the Valencia continental Basin to the north and
728 the Algerian and Ligurian oceanic Basins to the south and East. Contractional deformation of the Betic orogen
729 occurring during mid-Miocene times affected the Promontory at that time. The Messinian Salinity Crisis resulted
730 in an erosion of the margins and deposition of evaporites in the basins that are drawn on the map. The red
731 rectangle shows the location of the map figure 2.

732

733 Figure 2. Regional geological sketch of Ibiza Island and surrounding offshore. A) Geological map of Ibiza, with
734 zoom in on the NE part of the Island showing the location of the upper Miocene outcrops around Portinatx that
735 we studied. The offshore area displays the Present-day depth of the base of the Pliocene unit in meters. It
736 corresponds to the MES on the shelf. MSC related deposits (evaporites) are distinguished. B) Schematic cross-
737 section (from seismic data and bibliography) showing the relationship between the onshore study area and the
738 offshore known MSC markers in their geological context.

739

740 Figure 3. Map of the fold axes orientations in Unit 3, east of Portinatx; anticlinal and synclinal fold axes are
741 labeled. The fold axes orientations are grouped around 65°N and 140°N directions. Locations of the different
742 figures are indicated. Small stereographic projection of fold axes has been drawn with the *Stereonet* software
743 (Cardozo and Allmendiger, 2013).

744

745 Figure 4. Late Miocene series of the Cala de Serra, NE Ibiza. Unit 1 is a carbonate-rich unit assigned to
746 Tortonian - lower Messinian in age. This unit that overlaps mesozoïc recrystallized limestones is underlined by
747 eight meters of reworked corals (Porites rudstone) with benthic foraminifera and gastropods (section A).
748 Southward, near the main faults, these deposits change into detrital sedimentation composed of Mesozoic blocks.
749 Unit 2 is a detrital unit, with significant thickness decrease to the North. The size of the elements also decreases
750 progressively from very coarse elements (conglomerate) to the South (section A) to marls and clay-rich
751 sediments to the North (section C). This conglomerate-clay unit was set up by gravitational and fluvial processes
752 in the nearshore environment. Unit 2 is onlapped by oolite, microbialite, gastropod-rich limestones of Unit 3.
753 The lower part of Unit 3 (U3-1) is mainly composed of oolitic rich limestones indicating open shallow marine

environment dominated by tide dynamics. In the upper part of Unit 3 (U3-2), microbialites (thrombolite, stromatolite) become predominant and characterize the nearshore environment. The three stratigraphic logs show the faciologic variation in space and time of the tortono-messinian series along a SW-NE transect North of Cala de Serra. From section A to section C, the top of Unit 1 is located near the current sea surface. Unit 2 shows significant thickness reduction (25 m to 0.5 m) and lithological change (conglomerate dominant to marls dominant). Unit 3 reveals no significant lateral faciologic change but the top of this unit is eroded northward. At the SW all the Miocene series is overlap by the Margin Erosion Surface and overcome by Pliocene-Pleistocene formation.

Figure 5. a) Picture of Unit 3 (late Miocene series) along Aigua Blanca cliff, east of Portinatx. The lower part of the cliff (pink color, Unit 3-1) is composed of the herringbone layers (oolitic grainstones) that rest in an almost horizontal position when the upper part of the cliff (Unit 3-2) exhibits gentle folds; b) Line drawing of the structures. The outcrop length is 1.2 km when the maximum elevation of the cliff is 30 m. The base of Moscarter lighthouse appears on the left.

Figure 6. On Punta Galera Island, Unit 3 is folded in a large syncline trending N 175° (small stereographic projection) resting on the nearly flat Unit 1. A part of Unit 2 forms a wedge thickening to the west. The cliff is 25 m high. Unit 1 and 3 are made of limestones, while Unit 2 of white clay.

Figure 7. a and b) On the west side of the syncline, at the base of Unit 3, numerous load structures are observed sinking into the argillaceous sediments of Unit 2. They are elongated soft-sediment deformation structures and each long axis is orientated N0°, parallel to the syncline axis; c) Calcite geodes indicate the occurrence of fluid circulation in the lower part of Unit 3.

Figure 8. Cala Fondo outcrop. a) It is a large and flat syncline made of brecciated limestones resting on the top surface of Unit 1 (stereographic projection for fold axis); b) Unit 2 is less than one meter thick but is more developed on both the western and eastern sides of the syncline. The base of the black recrystallized limestones is broken by small extension fractures filled with red clays. Hikers for scale.

784 Figure 9. a) Picture of large-scale boudins formed in Unit 3, few meters east of the Moscarter lighthouse. The
785 cliff is 26 m high. The calcareous herringbone layers of Unit 3-1 are segmented in large rectangular boudins.
786 Around the blocks, deformation is limited to the corner parts where Unit 3-2 laminated upper layers form scar
787 folds composed of a tight syncline between two open anticlines; b) Line drawing of the picture; triangles indicate
788 the brecciated part of the layers; fold axis is drawn from the stereographic projection of Cardozo and
789 Allmendiger (2013); c) Brittle deformation of the laminated layers that have been transformed into recrystallized
790 limestone during diagenetic process. Small mode I fractures have been formed perpendicular to the layers and
791 they are filled with red argillaceous sediments. Fracture orientations range from N 125° to N 145°, parallel to the
792 fold axis; pen for scale.
793
794 Figure 10. Facies variations and diagenetic transformations in the upper part of Unit 3 below Moscarter
795 lighthouse. a-b) Unit 3-1 (lower part) is composed of oolitic grainstones with herringbone structures and trough
796 cross-stratification, while microbialites dominate limestone composition in the upper part (Unit 3-2).
797 Unit 3-2 shows the boundary between well preserved and diagenetically transformed (darkened part of figure b)
798 microbialitic facies. Laminations are visible (white lines). c,d,e) Neomorphic transformations of microbialitic
799 facies (Unit 3-2, darkened part picture b). c, d) Plain-polarized light (PPL) photomicrograph showing the original
800 texture and grain composition: microbial mat with abundant peloids. e) Cross-polarized light (CPL)
801 photomicrographs showing large-scale carbonate cement, a product of neomorphic changes.
802
803 Figure 11. a) West of Moscarter lighthouse, the herringbone layers (Unit 3-1) have been segmented in large
804 blocks while the microbialitic layers (Unit 3-2) have formed two half anticlines orientated N136° and N20°; b)
805 Line drawing of the picture showing the progressive onlap of paleosols that have filled the depression on top of
806 Unit 3; c) The small scale folds observed at the lower part of the eastern side have been estimated to have N105°
807 orientation; d) Extensive brittle deformation in the tilted layers of a scar fold.
808
809 Figure 12. East of Portinatx (location on Fig. 3 and Fig. 5), the onset of bedding tilt on the border of a large
810 boudin shows a large calcite wedge. The progressive increase of the layer tilting downward has opened the space
811 filled with vertical calcite crystals. Small stereographic projection indicates the construction of the fold axis.
812

Figure 13. Punta des Gat outcrop, a) Sections are composed of the upper part of Unit 1 and some strongly stretched layers of Unit 3; b) Depressions have formed at the surface of the late Miocene series (stretched layers of Unit 3 are in blue). Continental post Messinian sediments fill many of these depressions (Unit 4). The maximum elevation of the outcrop is 13 m.

Figure 14. Detail of the lower part of Unit 2 at Punta des Gat outcrop. This deformed formation is composed of mixed white and green clays, black recrystallized limestones, red blocks, and white clays, fragmented limestones and injected red clays that may come from the decalcification of limestone layers. The clays are a deformed part of Unit 2 and the limestones are the deformed and highly stretched part of the base of Unit 3. Notebook for scale.

Figure 15. From rectangular boudins to fishmouth boudins with an increasing ductility of the layers (a to c), redrawn from Wegmann (1932) and using parameters of Goscombe et al., (2004): L is long axis of boudin, W is thickness of boudinaged layer and N is the amount of dilatation.

Figure 16. Conceptual model of the large-scale boudinage of Unit 3 to form “chocolate tablets” in the late Miocene series of NE Ibiza. The herringbone layers of Unit 3-1 appear to be more competent and they form large scale rectangular boudins. On top of the boudins, the laminated layers of Unit 3-2 are bent to form passive folds. Sliding over the ductile clayey layers of Unit 2 has shifted the boudins. Rectangular boudins have been formed to the west and progressively a more diffuse stretching of the layers is observed to the east. a) Base of the boudins as they can be seen in Punta Galera outcrop (Fig. 6); b) Large blocks separated by a tight syncline and the progressive onlap of paleosols filling the depression (Fig. 11); c) Extensional deformation and progressive tilting of the laminated layers forming calcite crystal wedges (Fig. 9); d) The strongly stretched part of Unit 3 resting on Unit 1 flat top; there, the two units are separated by clays that may be considered as coming from decalcified limestones (Fig. 13). The continental post-Messinian sediments (Unit 4) have filled many of the depressions formed by the stretching of Unit 3. U1, U2, U3, and U4 refer to the different sedimentary units.

Figure 17. Schematic map of Portinatx area. Blocks edges are figured by black segments. The length of the boudins (L) is drawn in red when measured in the WSW-ENE direction (red circles) and green in the NW-SE direction (green stars). The boudins are longer in the WSW-ENE direction.

843 Table 1. Microthermometric data of fluid inclusions in calcite crystals. The trapping conditions are reconstructed
844 from the homogenization temperatures. Samples coming from the Cala de Ponent indicate calcite crystals
845 formation between 190 and 260°C. Temperatures are given with an accuracy of 1.0°C.
846

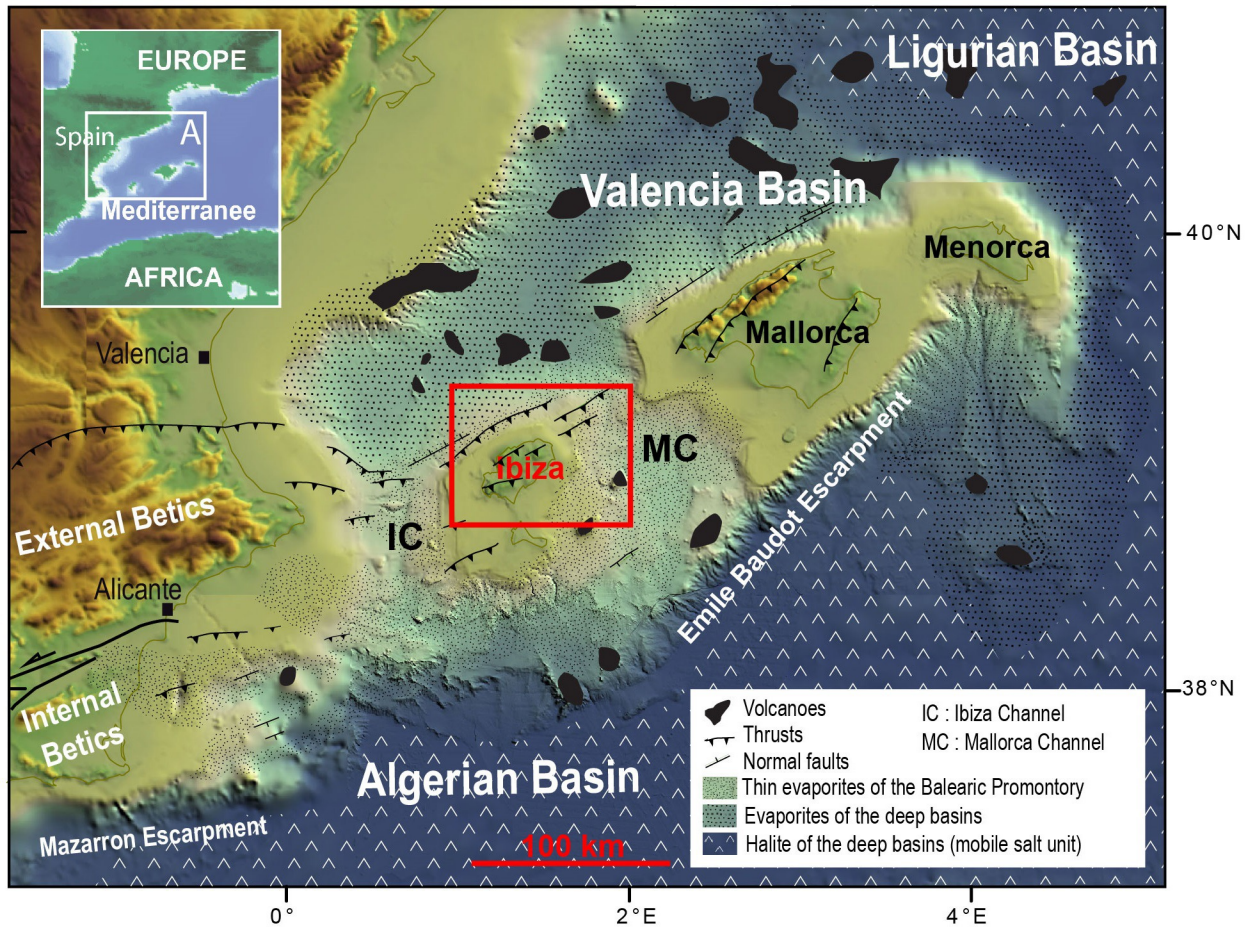
EUROPE
Spain
A
Mediterranee
AFRICA
Ligurian Basin
Valencia Basin
Menorca
Mallorca
Valencia
Ibiza
MC
IC
External Betics
Alicante
Emile Baudot Escarpment
Internal Betics
Algerian Basin
Mazarron Escarpment
100 km
40°N
38°N
0°
2°E
4°E
Volcanoes
Thrusts
Normal faults
IC : Ibiza Channel
MC : Mallorca Channel
Thin evaporites of the Balearic Promontory
Evaporites of the deep basins
Halite of the deep basins (mobile salt unit)

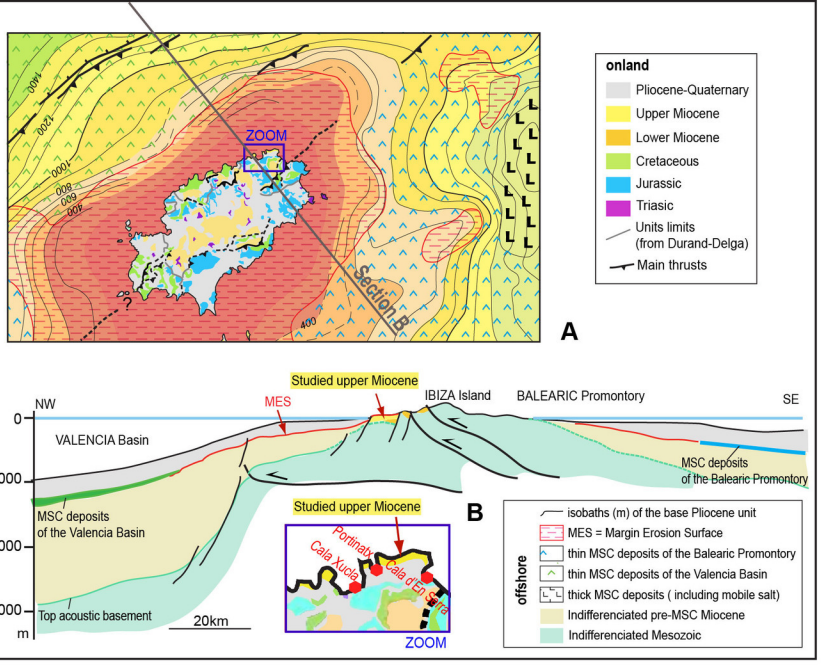
ZOOM
Section B
A
onland
Pliocene-Quaternary
Upper Miocene
Lower Miocene
Cretaceous
Jurassic
Triasic
Units limits
(from Durand-Delga)
Main thrusts
Studied upper Miocene
NW
MES
IBIZA Island
BALEARIC Promontory
SE
0
1000
2000
3000
m
VALENCIA Basin
MSC deposits
of the Balearic Promontory
MSC deposits
of the Valencia Basin
Top acoustic basement
20km
B
Studied upper Miocene
Portinatx
Cala Xuclar
Cala d'En Serra
ZOOM
offshore
isobaths (m) of the base Pliocene unit
MES = Margin Erosion Surface
thin MSC deposits of the Balearic Promontory
thin MSC deposits of the Valencia Basin
thick MSC deposits (including mobile salt)
Indifferenciated pre-MSC Miocene
Indifferenciated Mesozoic

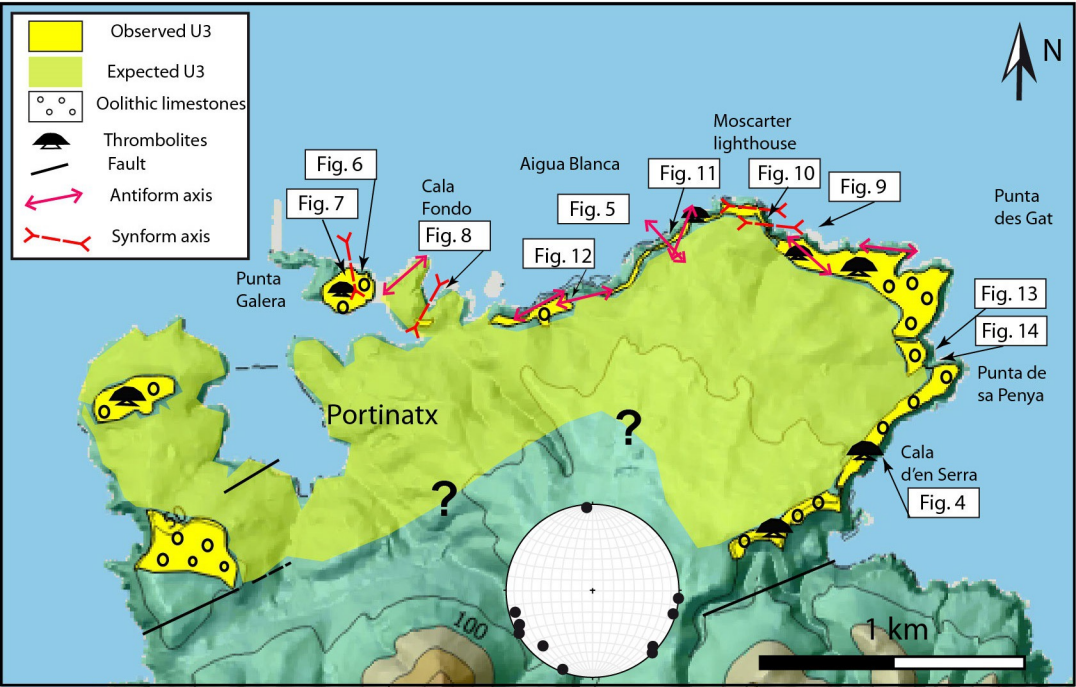
Observed U3
Expected U3
Oolithic limestones
Thrombolites
Fault
Antiform axis
Synform axis
N
Fig. 6
Fig. 7
Fig. 8
Cala Fondo
Aigua Blanca
Fig. 5
Fig. 12
Fig. 11
Fig. 10
Moscarter lighthouse
Fig. 9
Punta des Gat
Punta Galera
Fig. 13
Fig. 14
Punta de sa Penya
Portinatx
?
?
Cala d'en Serra
Fig. 4
100
1 km

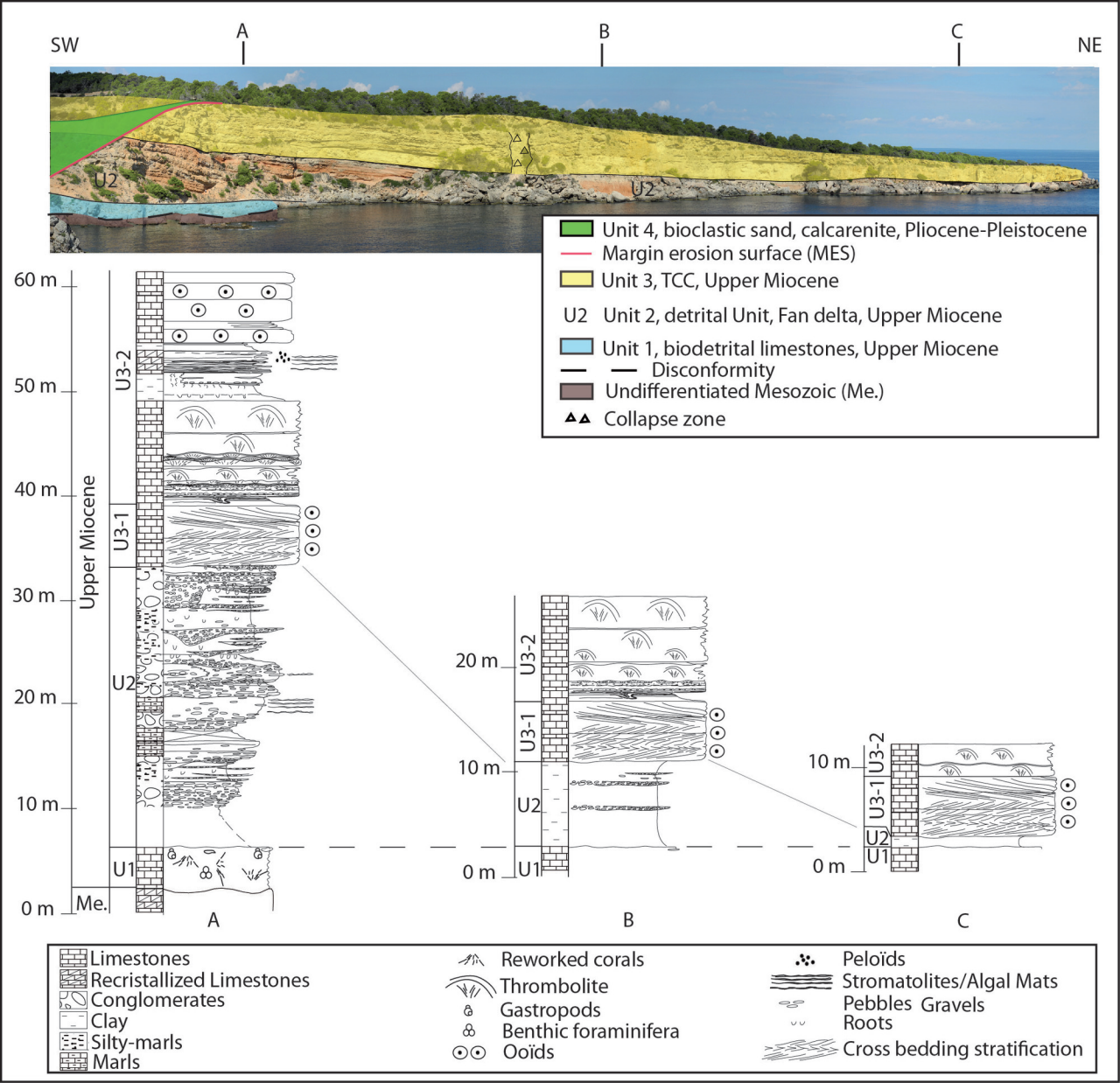
SW
A
B
C
NE
U2
U2
Unit 4, bioclastic sand, calcarenite, Pliocene-Pleistocene
Margin erosion surface (MES)
Unit 3, TCC, Upper Miocene
U2 Unit 2, detrital Unit, Fan delta, Upper Miocene
Unit 1, biodetrital limestones, Upper Miocene
Disconformity
Undifferentiated Mesozoic (Me.)
Collapse zone
60 m
50 m
40 m
30 m
20 m
10 m
0 m
Upper Miocene
U3-2
U3-1
U2
U1
Me.
A
20 m
10 m
0 m
B
C
Limestones
Recristallized Limestones
Conglomerates
Clay
Silty-marls
Marls
Reworked corals
Thrombolite
Gastropods
Benthic foraminifera
Ooïds
Peloïds
Stromatolites/Algal Mats
Pebbles Gravels
Roots
Cross bedding stratification

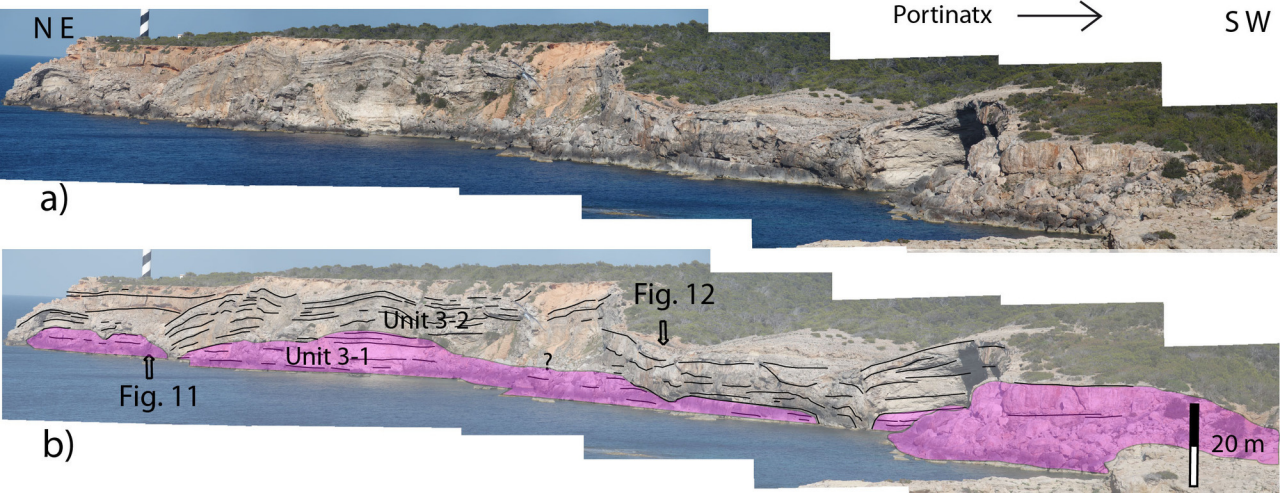
N E
Portinatx
S W
a)
Fig. 12
Unit 3-2
Unit 3-1
?
Fig. 11
b)
20 m

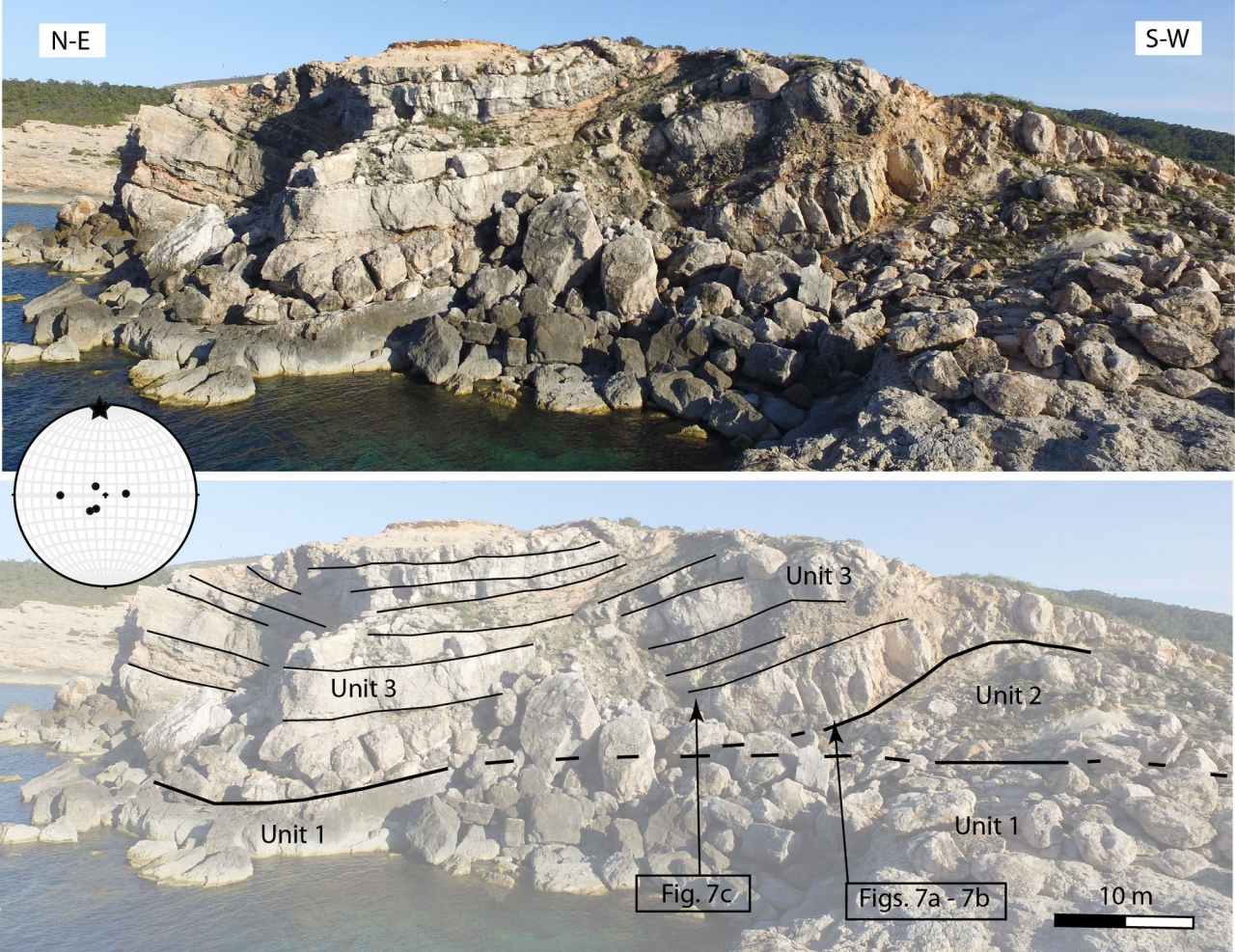
N-E
S-W
Unit 3
Unit 3
Unit 2
Unit 1
Unit 1
Fig. 7c
Figs. 7a - 7b
10 m

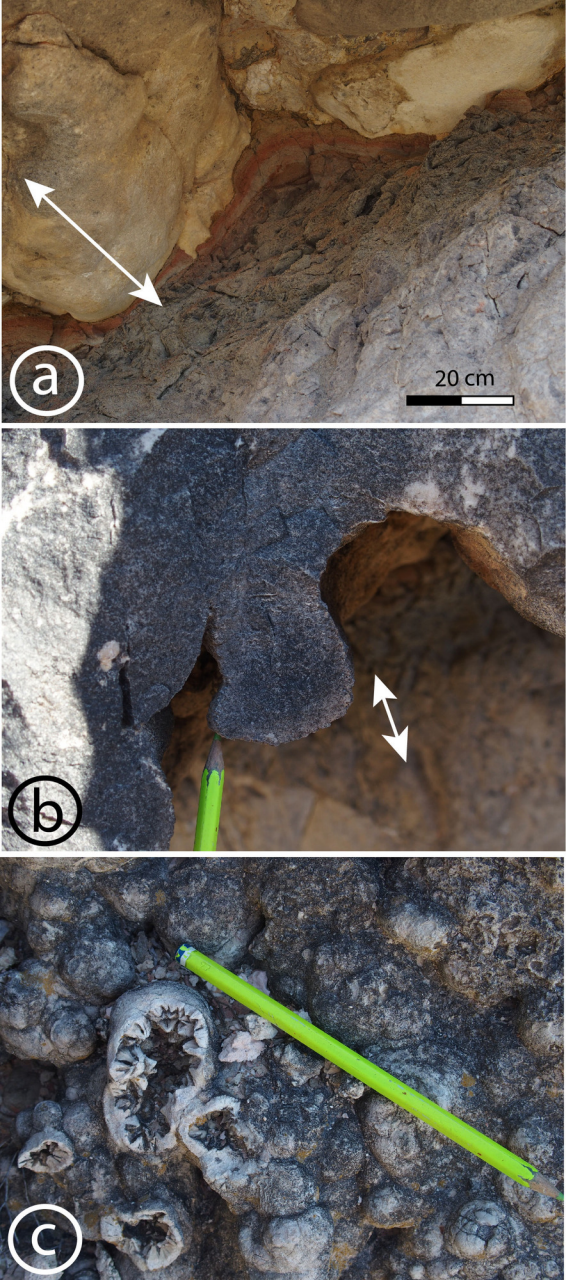
a
20 cm
b
c


E
W
a)
Brecciated limestones
Unit 2
Unit 2
Unit 1
b)
Unit 1

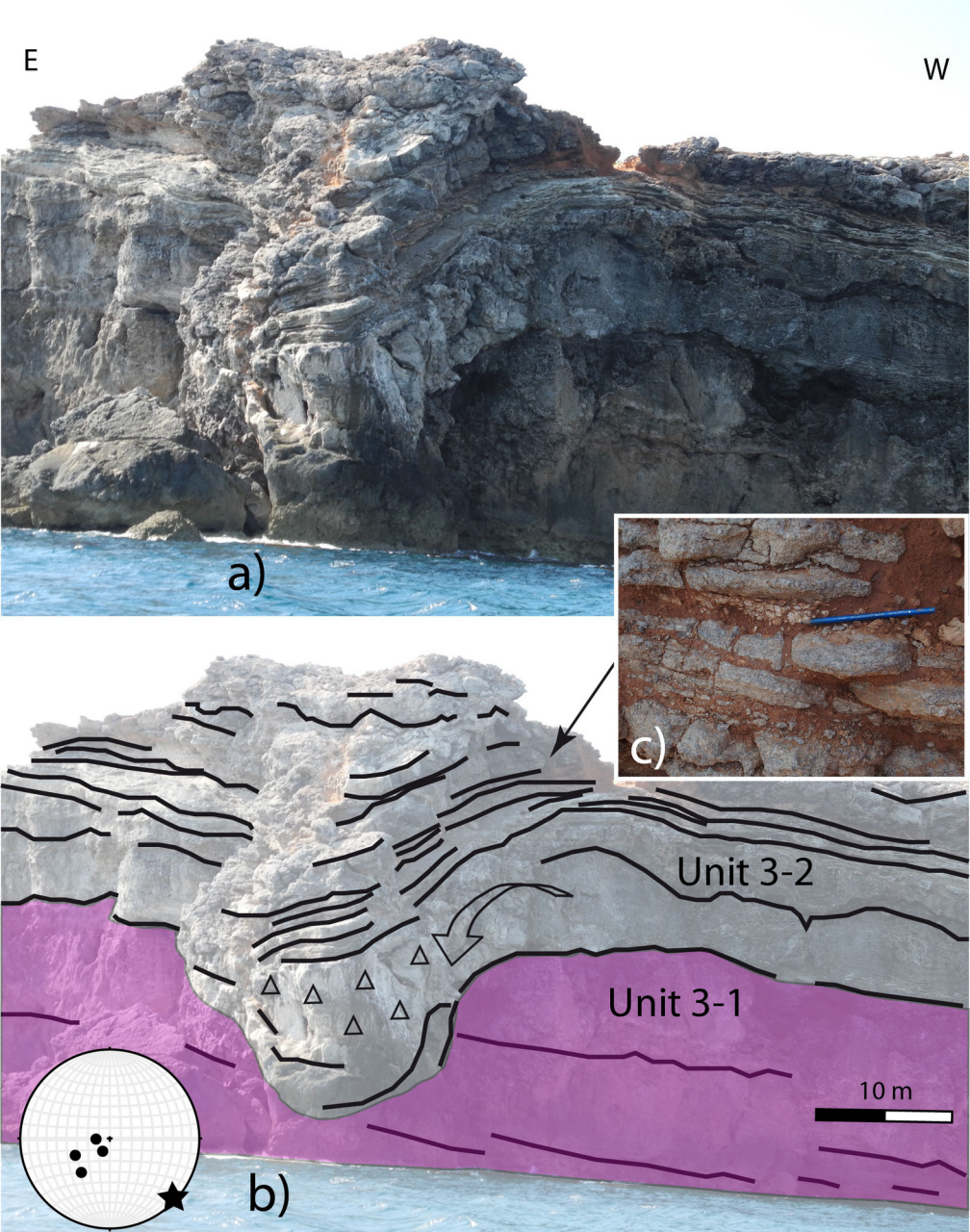
E
W
a)
c)
Unit 3-2
Unit 3-1
10 m
b)

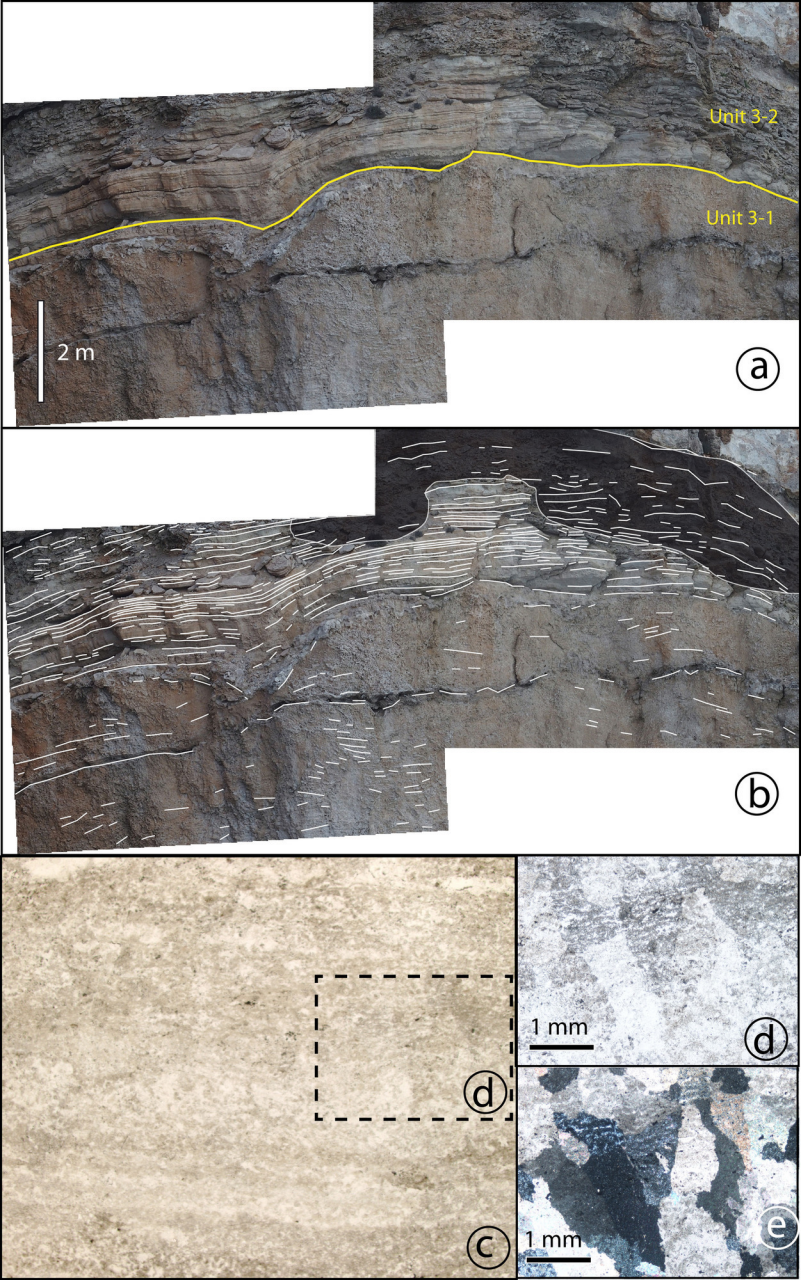
Unit 3-2
Unit 3-1
2 m
a
b
d
c
1 mm
d
1 mm
e

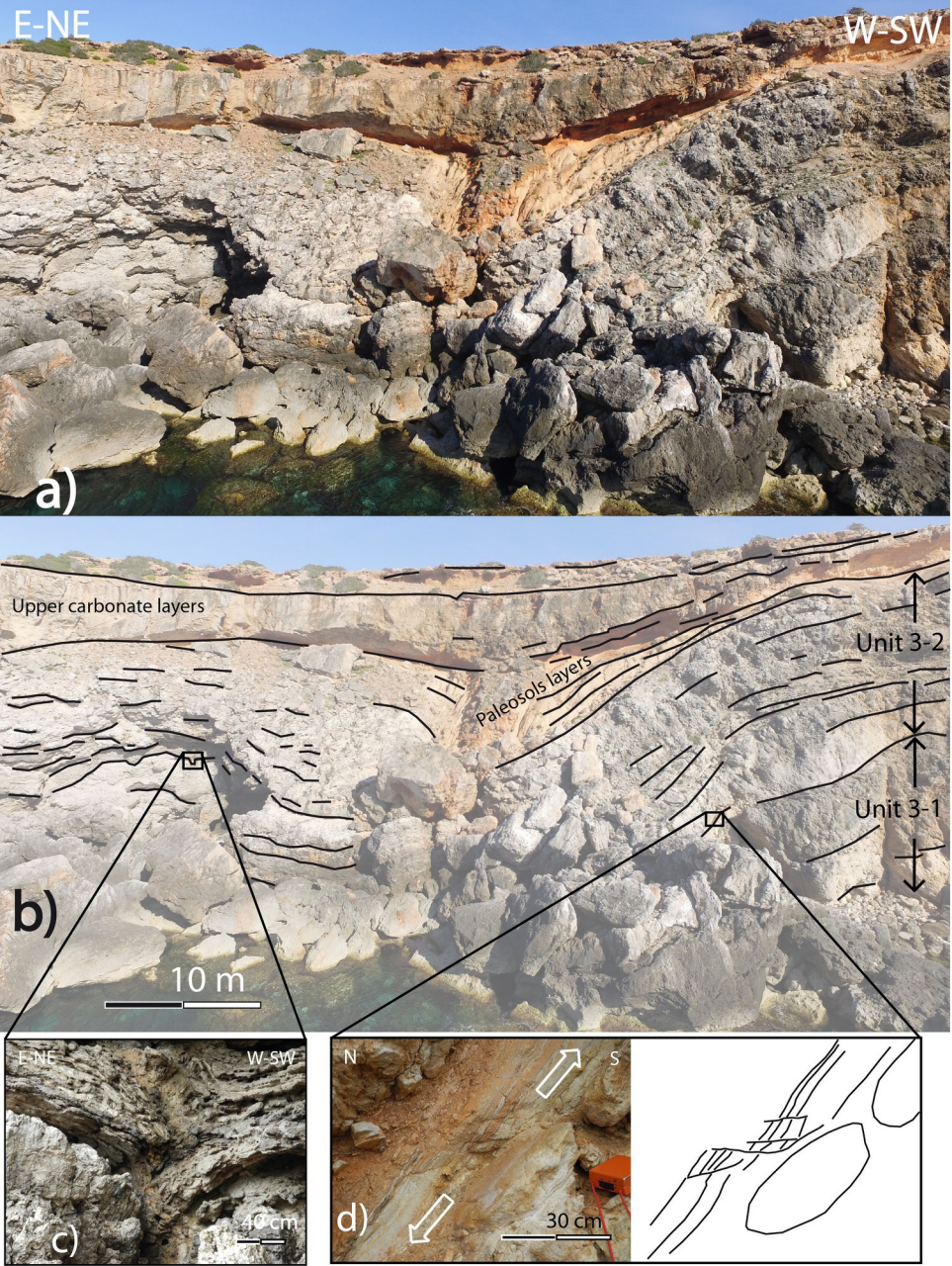
E-NE
W-SW
a)
Upper carbonate layers
Paleosols layers
Unit 3-2
Unit 3-1
b)
10 m
E-NE
W-SW
40 cm
c)
N
S
30 cm
d)

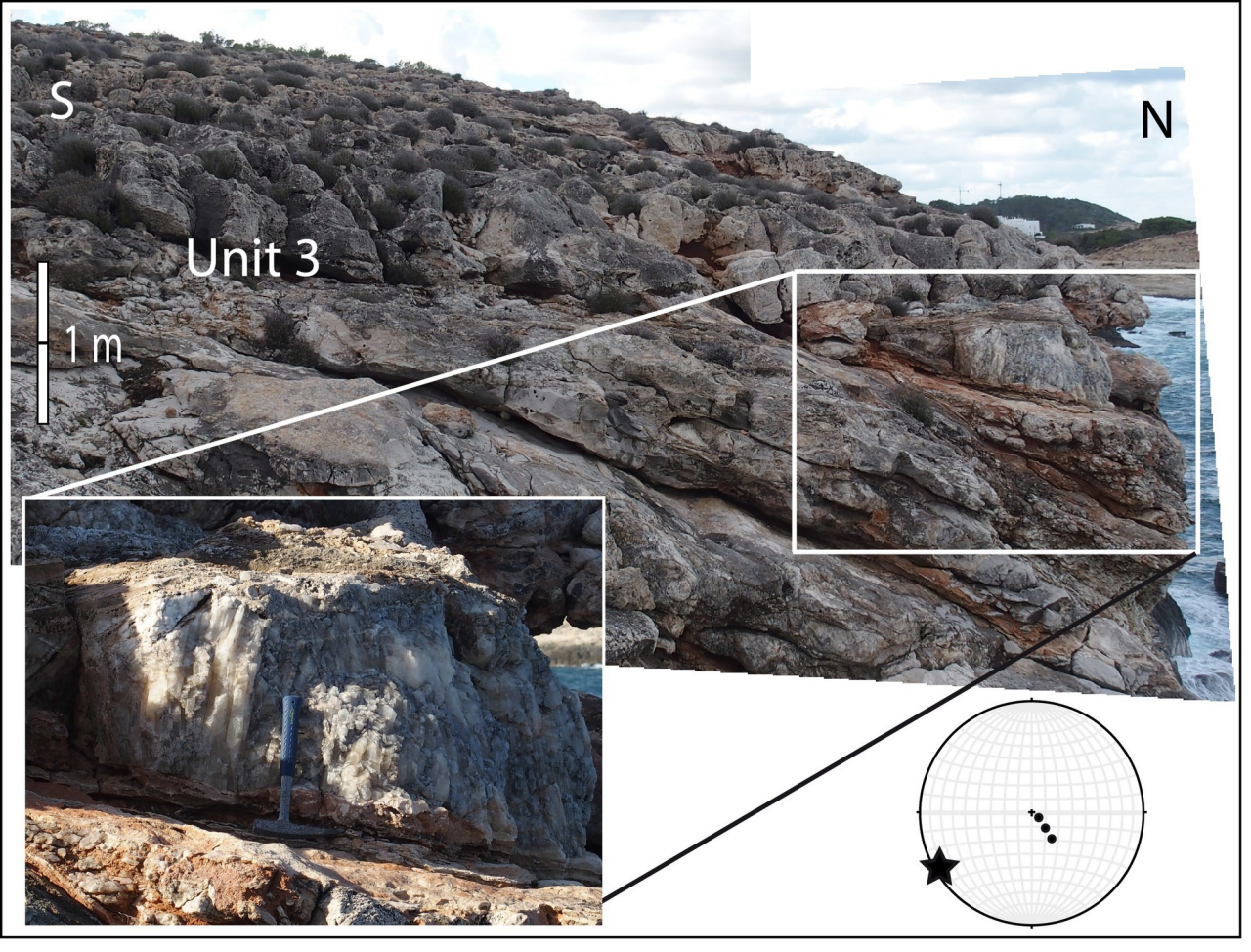
S
N
Unit 3
1 m

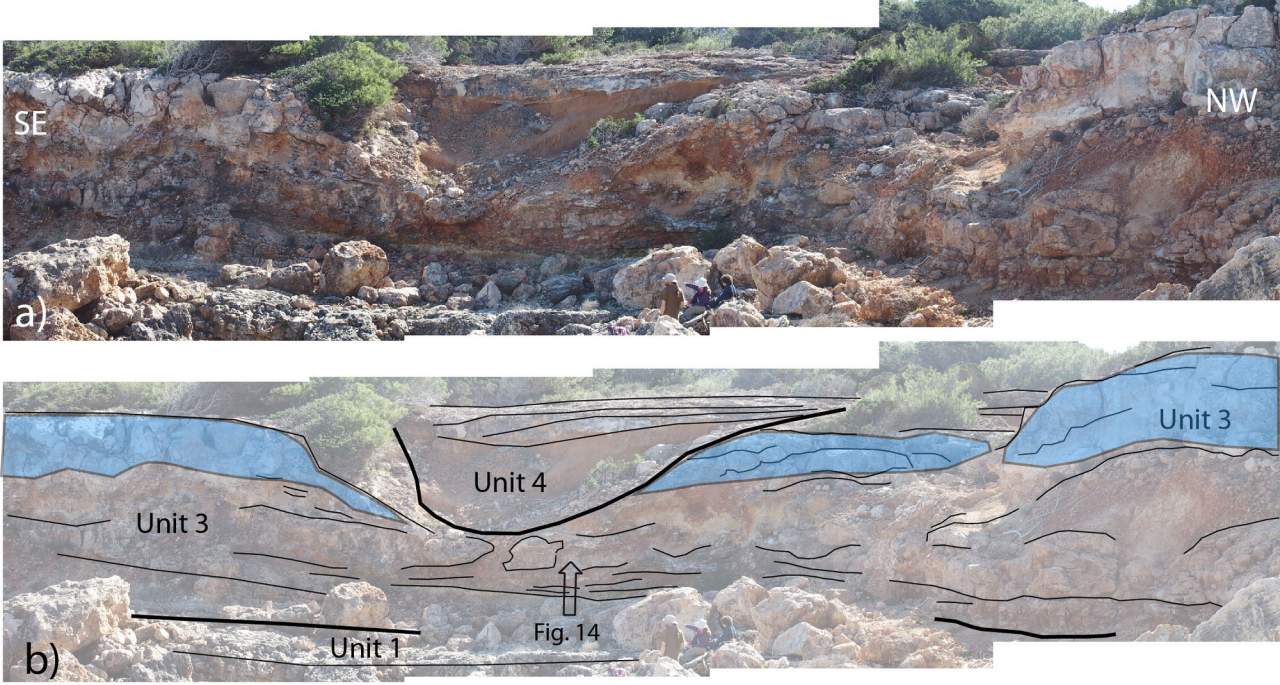
SE
NW
a)
Unit 3
Unit 4
Unit 3
Unit 1
Fig. 14
b)

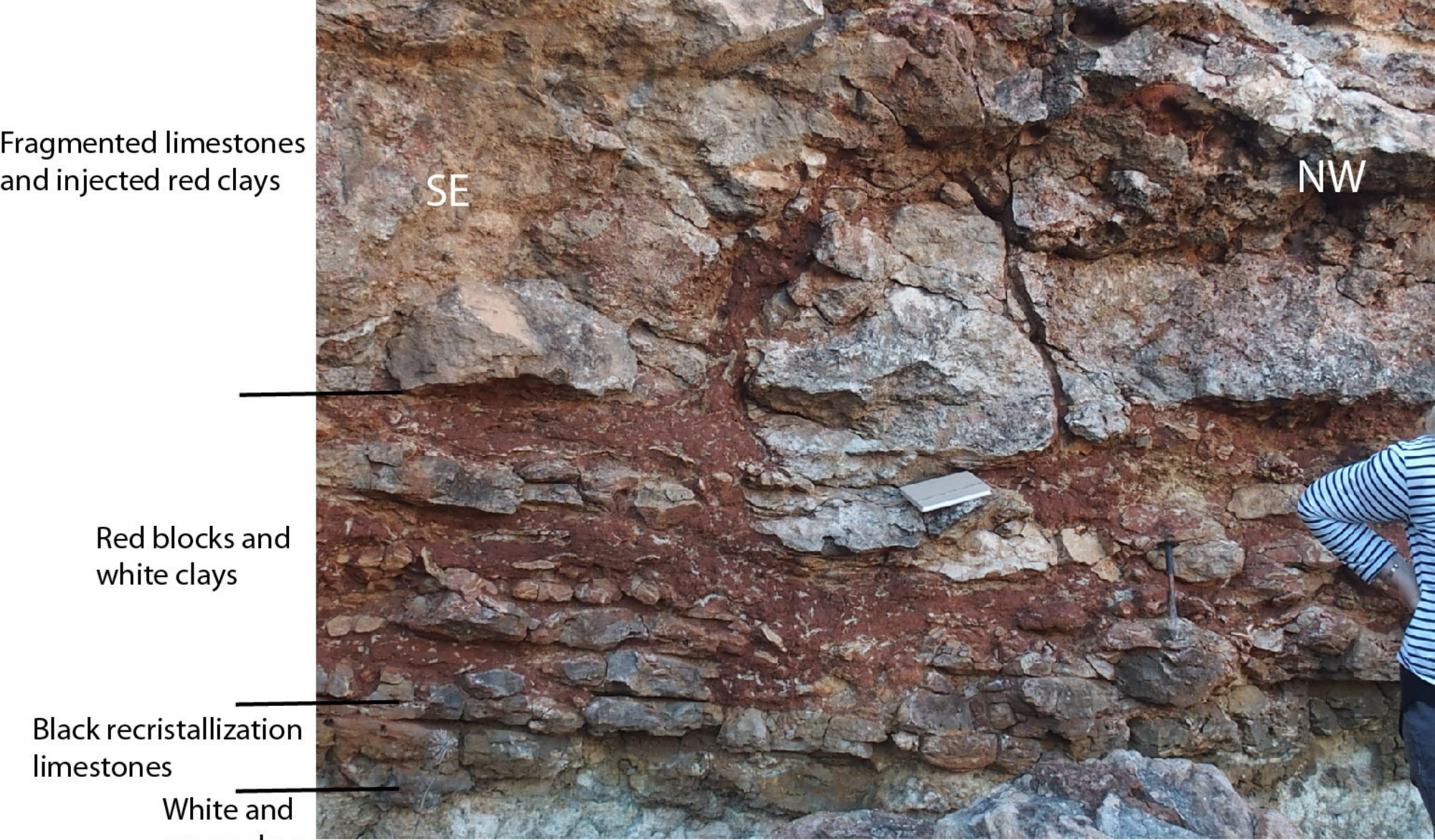
Fragmented limestones and injected red clays
SE
NW
Red blocks and white clays
Black recristallization limestones
White and green clays

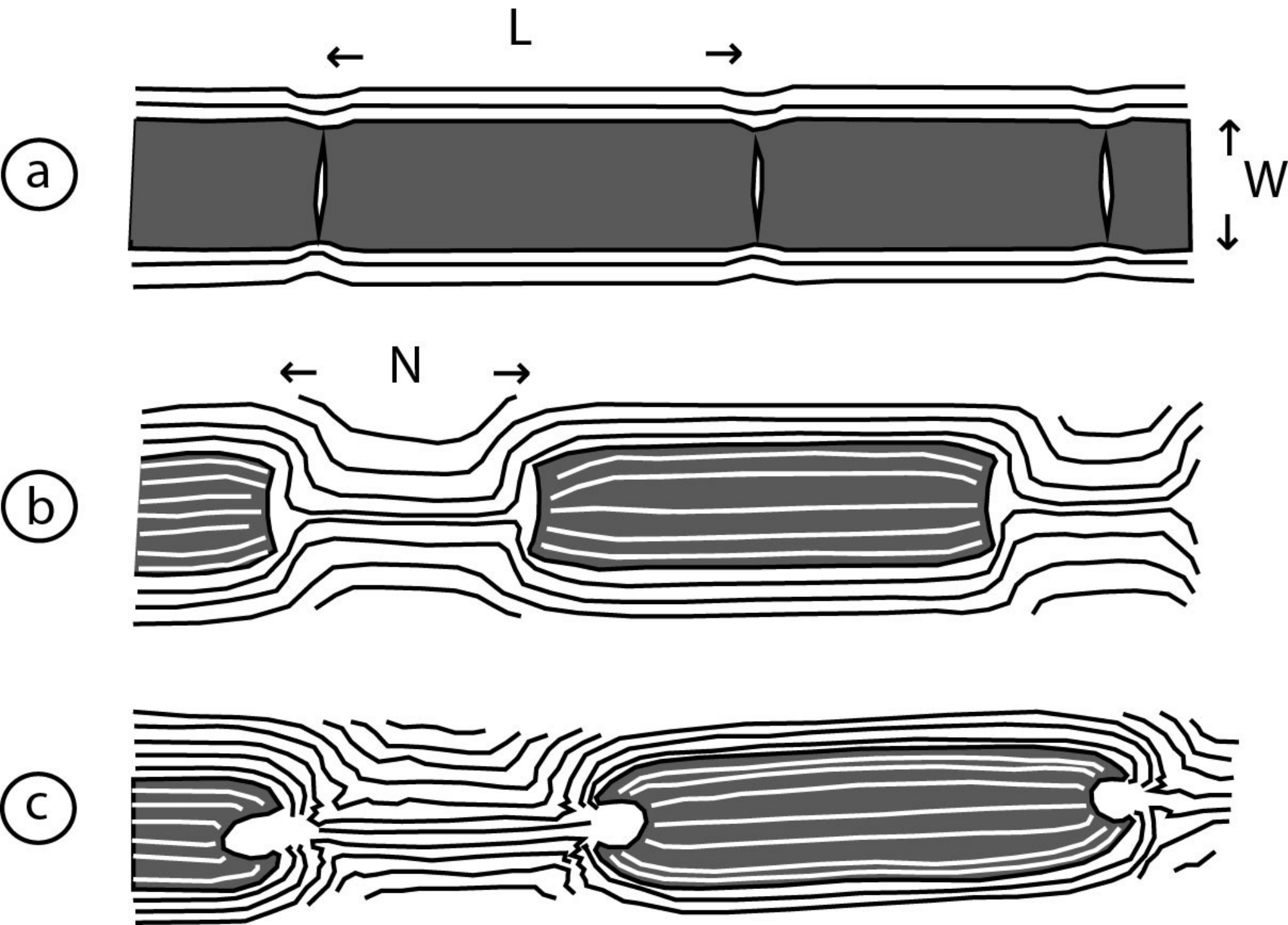
L
a
W
N
b
c

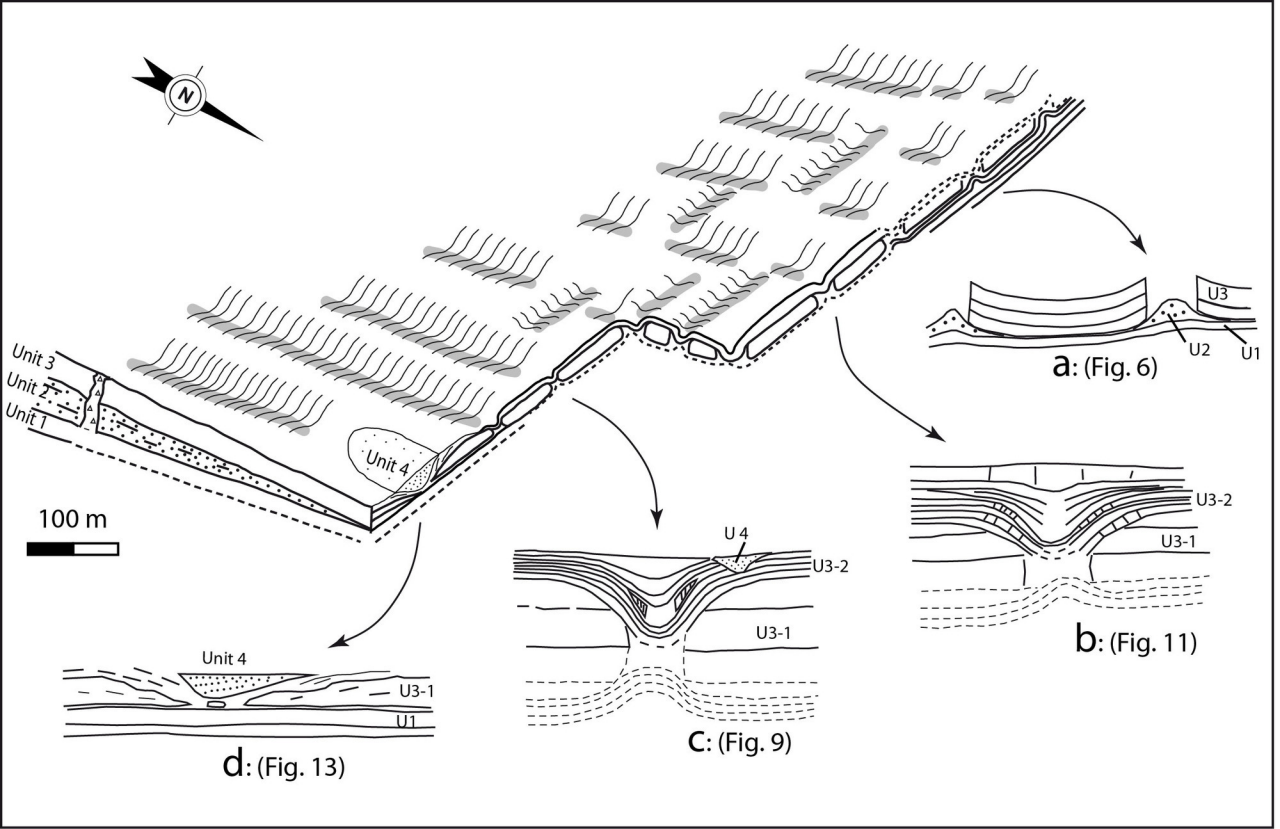
N
Unit 3
Unit 2
Unit 1
Unit 4
100 m
U3
U2
U1
a: (Fig. 6)
U3-2
U3-1
b: (Fig. 11)
U 4
U3-2
U3-1
c: (Fig. 9)
Unit 4
U3-1
U1
d: (Fig. 13)

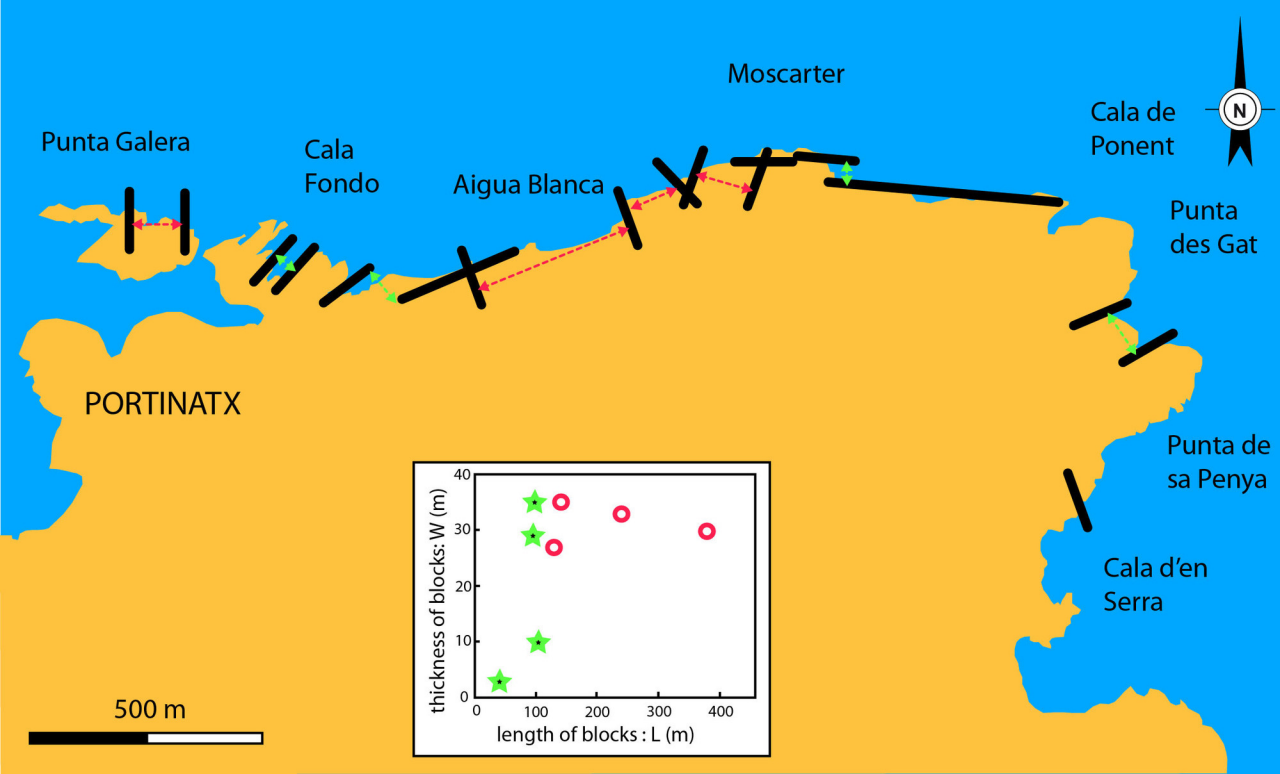
Moscarter
Punta Galera
Cala
Fondo
Aigua Blanca
Cala de
Ponent
N
Punta
des Gat
PORTINATX
Punta de
sa Penya
Cala d'en
Serra
500 m
thickness of blocks: W (m)
length of blocks : L (m)
0
10
20
30
40
0
100
200
300
400

samples	**PO1**	**PO2**
homogenization temperature	219	188
	242	190
	256	202
	257	205
	260	209
	260	
	260	